NASA/TM–2016-218978

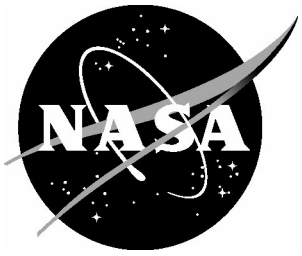

Ultrasonic Nondestructive Evaluation of Pultruded Rod Stitched Efficient Unitized Structure (PRSEUS) During Large-Scale Load Testing and Rod Push-Out Testing

Patrick H. Johnston and Peter D. Juarez
Langley Research Center, Hampton, Virginia 23681

May 2016

NASA STI Program . . . in Profile

Since its founding, NASA has been dedicated to the advancement of aeronautics and space science. The NASA scientific and technical information (STI) program plays a key part in helping NASA maintain this important role.

The NASA STI program operates under the auspices of the Agency Chief Information Officer. It collects, organizes, provides for archiving, and disseminates NASA's STI. The NASA STI program provides access to the NTRS Registered and its public interface, the NASA Technical Reports Server, thus providing one of the largest collections of aeronautical and space science STI in the world. Results are published in both non-NASA channels and by NASA in the NASA STI Report Series, which includes the following report types:

- TECHNICAL PUBLICATION. Reports of completed research or a major significant phase of research that present the results of NASA Programs and include extensive data or theoretical analysis. Includes compilations of significant scientific and technical data and information deemed to be of continuing reference value. NASA counter-part of peer-reviewed formal professional papers but has less stringent limitations on manuscript length and extent of graphic presentations.

- TECHNICAL MEMORANDUM. Scientific and technical findings that are preliminary or of specialized interest, e.g., quick release reports, working papers, and bibliographies that contain minimal annotation. Does not contain extensive analysis.

- CONTRACTOR REPORT. Scientific and technical findings by NASA-sponsored contractors and grantees.

- CONFERENCE PUBLICATION. Collected papers from scientific and technical conferences, symposia, seminars, or other meetings sponsored or co-sponsored by NASA.

- SPECIAL PUBLICATION. Scientific, technical, or historical information from NASA programs, projects, and missions, often concerned with subjects having substantial public interest.

- TECHNICAL TRANSLATION. English-language translations of foreign scientific and technical material pertinent to NASA's mission.

Specialized services also include organizing and publishing research results, distributing specialized research announcements and feeds, providing information desk and personal search support, and enabling data exchange services.

For more information about the NASA STI program, see the following:

- Access the NASA STI program home page at http://www.sti.nasa.gov

- E-mail your question to help@sti.nasa.gov

- Phone the NASA STI Information Desk at 757-864-9658

- Write to:
  NASA STI Information Desk
  Mail Stop 148
  NASA Langley Research Center
  Hampton, VA 23681-2199

NASA/TM–2016-218978

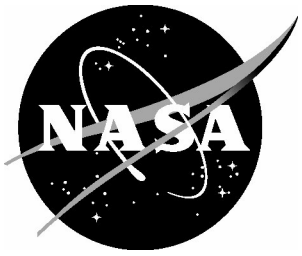

Ultrasonic Nondestructive Evaluation of Pultruded Rod Stitched Efficient Unitized Structure (PRSEUS) During Large-Scale Load Testing and Rod Push-Out Testing

Patrick H. Johnston and Peter D. Juarez
Langley Research Center, Hampton, Virginia 23681

National Aeronautics and
Space Administration

Langley Research Center
Hampton, Virginia 23681-2199

May 2016

Available from:

NASA STI Program / Mail Stop 148
NASA Langley Research Center
Hampton, VA 23681-2199
Fax: 757-864-6500

ABSTRACT

The Pultruded Rod Stitched Efficient Unitized Structure (PRSEUS) is a structural concept developed by the Boeing Company to address the complex structural design aspects associated with a pressurized hybrid wing body (HWB) aircraft configuration. The HWB has long been a focus of NASA's environmentally responsible aviation (ERA) project, following a building block approach to structures development, culminating with the testing of a nearly full-scale multi-bay box (MBB), representing a segment of the pressurized, non-circular fuselage portion of the HWB. PRSEUS is an integral structural concept wherein skins, frames, stringers and tear straps made of a variable number of layers of dry warp-knit carbon-fiber stacks are stitched together, then resin-infused and cured in an out-of-autoclave process. The PRSEUS concept has the potential for reducing the weight and cost and increasing the structural efficiency of transport aircraft structures. A key feature of PRSEUS is the crack-arresting nature of the stitches, which enables the use of fail-safe design principles. During the load testing of the MBB, ultrasonic NDE was used to monitor several sites of intentional barely-visible impact damage (BVID) as well as to survey the areas surrounding the failure cracks after final loading to catastrophic failure.

In parallel with the large-scale structural testing of the MBB, mechanical tests were conducted of the PRSEUS rod-to-overwrap bonds, as measured by pushing the rod axially from a short length of stringer. Ultrasonic NDE was used to screen the rod specimens for existing flaws before push-out testing and to measure the extent of impact damage inflicted prior to push-out testing.

1.0 Introduction

The Hybrid Wing-Body (HWB) Multi-Bay Test [1] is a joint development effort between the Boeing Company and NASA Langley Research Center, sponsored in part by the Environmentally Responsible Aviation (ERA) Project and Boeing internal R&D. The HWB concept is also sometimes referenced as the Blended Wing Body (BWB) concept. The fabrication of the MBB is described in detail in the final report from Boeing [2]. This Technical Memorandum (TM) presents the results of ultrasonic inspections in support of the HWB Multi-Bay Test, and is a companion document with the NASA test and analysis reports [3-4], reports on acoustic emission and fiber optic strain measurements performed during the test [5-6], and other mechanical tests [7-9]. This paper also includes NDE of specimens for a study of the shear strength of bond between the pultruded rods and the overwrapping fabric, which is described in greater detail in a companion TM [8].

2.0 Background

2.1 Pultruded Rod Stitched Efficient Unitized Structure (PRSEUS) Concept

The PRSEUS concept, depicted in Fig. 1, has been developed as a low-cost, lightweight composite structure for aircraft [10-11], which offers advantages over traditional metallic structure. The PRSEUS concept is comprised of a stitched carbon-epoxy material system with the potential for reducing the weight and cost of transport aircraft structure by eliminating fasteners, thereby reducing part count and labor. By adding unidirectional carbon rods to the top of stiffeners, the panel becomes more structurally efficient. This combination produces a more damage tolerant design.

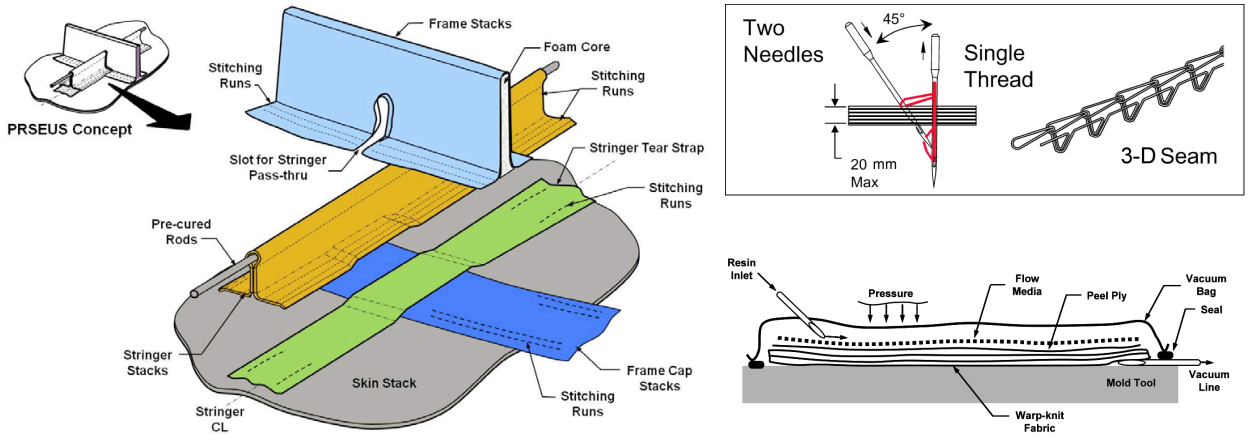

FIGURE 1. The PRSEUS dry preform is built up from carbon fabric stacks for the frame, stringers and skin. The layers are stitched together with Vectran fibers, using a single-sided sewing method, then bagged and infused with resin [10].

Some key features of the PRSEUS concept are: the improved stiffness provided by the pultruded rod; the crack-arresting nature of the stitches, which enables the use of failsafe design principles; reduced tooling size and weight enabled by the self-supporting nature of the stitched preform; and improved resin infusion through the use of Controlled Atmospheric Pressure Resin Infusion (CAPRI). A photograph of the stiffener side of a flat PRSEUS test panel is shown in Fig. 2 [10].

Figure 2. An example of a PRSEUS panel. This particular flat panel comprises four frames and seven stringers [10].

2.2 Ultrasonic Measurement Methods

2.2.1 Phased Array Inspection on Flat and Cylinrical Surfaces

Interrogation of the PRSEUS specimens was performed using normal-incidence phased array ultrasonic techniques (PAUT). The arrays were commercial 64-element (each 0.4” x 0.02”), 10 MHz linear arrays, either mounted on a solid plastic 0° wedge (for flat surfaces) or in a water-filled housing with rubber membrane (for curved surfaces or surfaces with strain gages and their associated wiring installed for test) [12]. A spray of water on the panel surface served as ultrasonic couplant. Effective apertures comprising groups of 16 adjacent elements were electronically scanned by 1-element spacing along the length of the array, and the probe was mounted to a manual X-Y manual scanner for positioning, as shown in Fig.3. Pulse-echo signals were measured at each position over the scanned area of up to 20” x 20”.

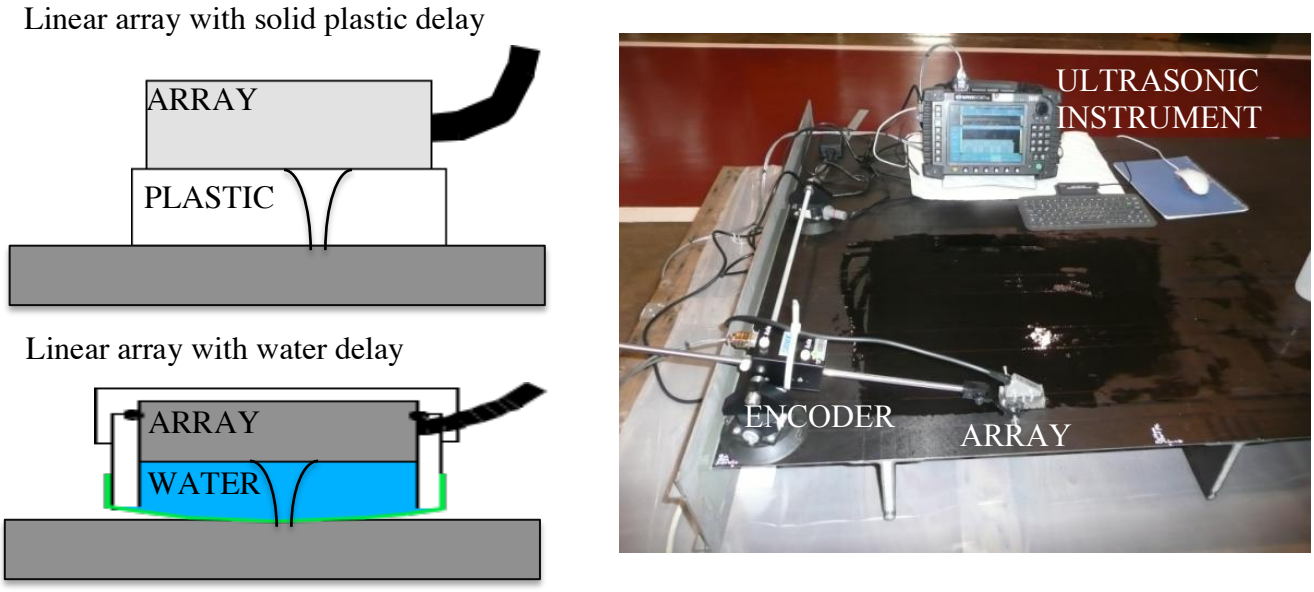

FIGURE 3. A linear ultrasonic array coupled to a manual X-Y encoder was used to interrogate PRSEUS panels. On flat panels, without gages, a solid plastic wedge was used. In order to better accommodate the presence of wires, gages, and tape, a captive water column with flexible face was used after panel instrumentation. The captive water probe was also used on the curved panel.

2.2.2 Curved Phased Array Probe for Stiffener Rods and Frame Caps

Part of the HWB Multi-Bay Test calls for inspection of a rod and a frame before and after induction of barely visible impact damage. In order to scan these locations, a captive water probe similar to that depicted in Fig. 3 was designed to couple a curved linear array to the rod or frame tip. A depiction of the curved array probe inspecting a rod is presented in Fig. 4.

2.2.3 Immersion Scans of Stiffener Rods

The rod specimens for the rod push-out test were inspected in an immersion scanner using a turntable for angular positioning and a Z-axis linear stage to scan a 0.5 inch diameter, 2.0 inch focal length, 10 MHz transducer along the length of the rod. A photograph of a rod specimen mounted in the scanning tank is presented in Fig. 5. The rod specimens were mounted on an immersed turntable, with the rod centered on the turntable axis, to provide angular positioning. A transducer on a vertical linear stage scanned the length of the rod.

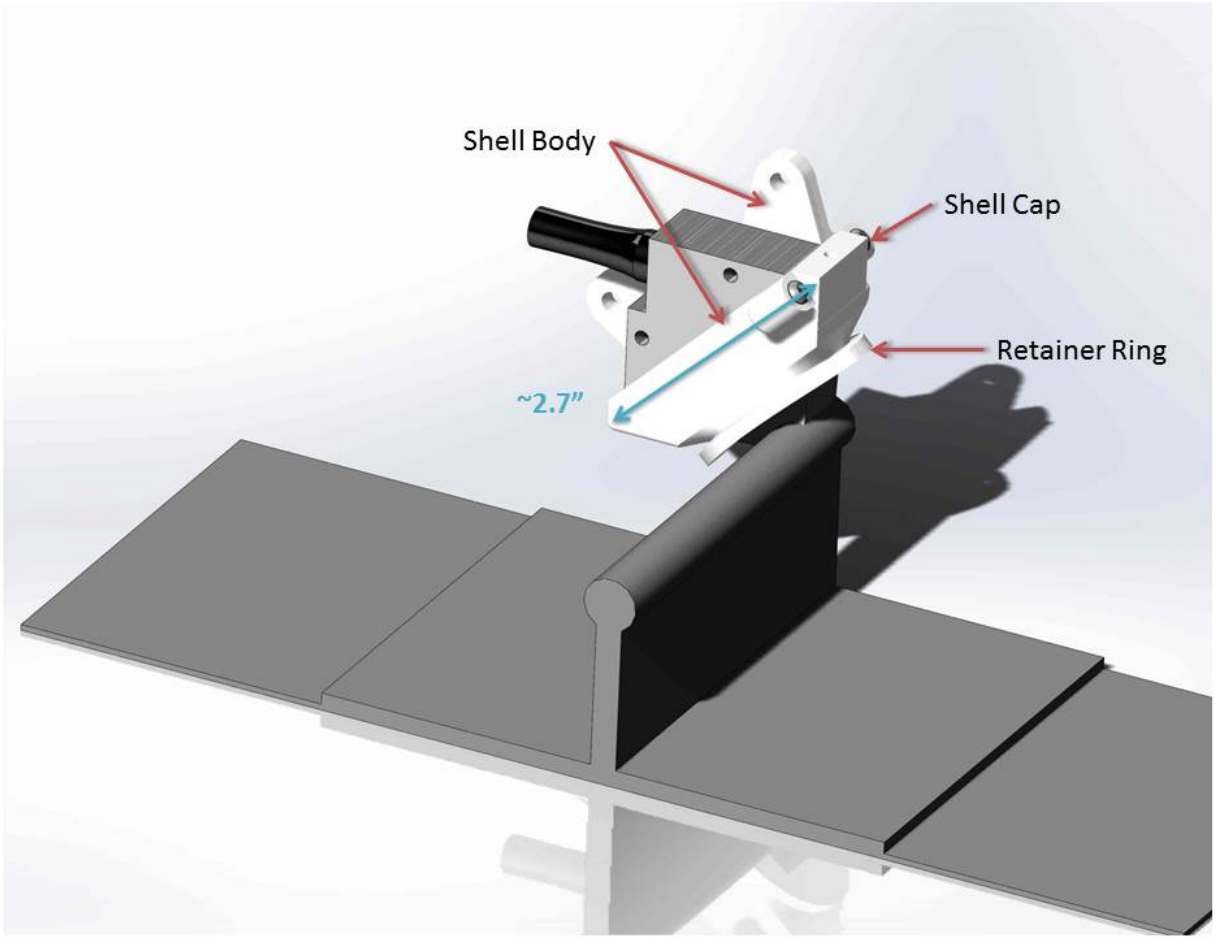

FIGURE 4. A captive water column probe was designed to position a curved array probe over the rod and frame tip impact sites.

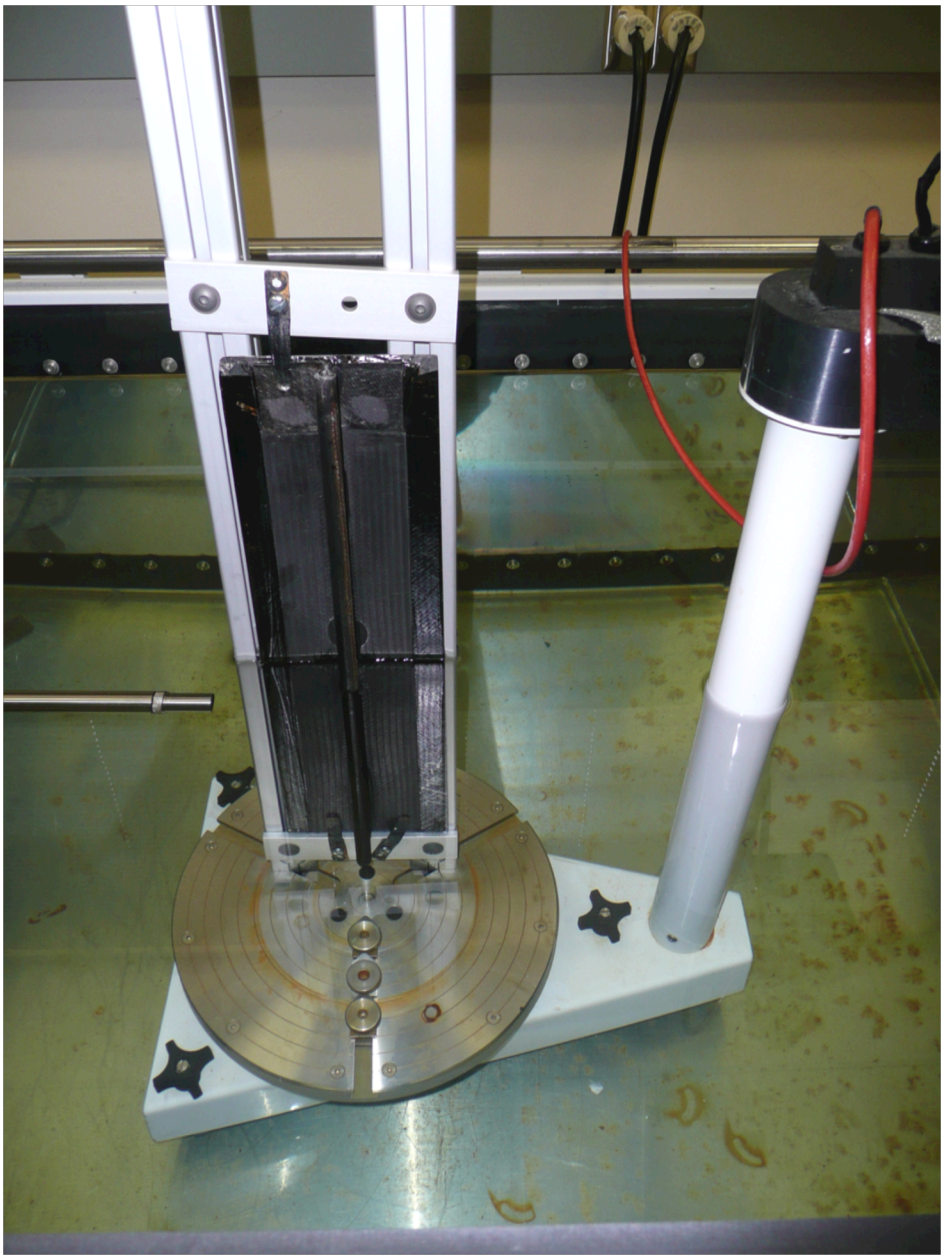

FIGURE 5. The rod specimens were mounted on an immersed turntable, with the rod centered on the turntable axis, to provide angular positioning. A transducer on a vertical linear stage scanned the length of the rod.

2.3 Previous Tests

Previous studies produced ultrasonic results from three different PRSEUS test articles: a flat, 7-stringer and 4-frame panel, loaded in compression first statically, then cyclically [12-13]; a curved, 7-stringer and 5-frame panel, loaded in axial tension and pressure with reactive edge loads [14]; and a cube, comprising six flat PRSEUS panels joined via integral caps along their edges, loaded in pressure, ultimately to catastrophic failure [10-11, 13, 15]. Ultrasonic measurement of rod/overwrap bonds were performed in support of a separate earlier study [16].

2.3.1 Flat 7-Stringer Panel

The results for this panel were previously reported at the 2010 Review of Progress in Quantitative Nondestructive Evaluation (QNDE) conference [12]. Figure 6 presents the PAUT pulse-echo C-scan results at various stages of the test. The grayscale represents the signal amplitude at the depth corresponding to the back surface of the free skin, so the back surface of the skin is gray, while the thicker flange regions are darker. Panels 6(a) and 6(b) show scans of the impact area before and after impact, respectively. A delamination is observed between the skin plies and the underlying flange plies, which runs vertically approximately 4” above and 4” below the impact point, while being held constrained in the horizontal direction by the first line of stitches encountered.

Figure 6(c) shows the C-scan obtained after the panel was loaded in static compression to its design limit load of 137,000 pounds. The dimensions of the delamination remained unchanged. Figure 6(d) presents the C-scan obtained after the panel was subjected to 20 cycles of compression up to 96,000 pounds. Again, the dimensions of the delamination at the BVID point remained unchanged.

(a) C-scan Pre-Impact

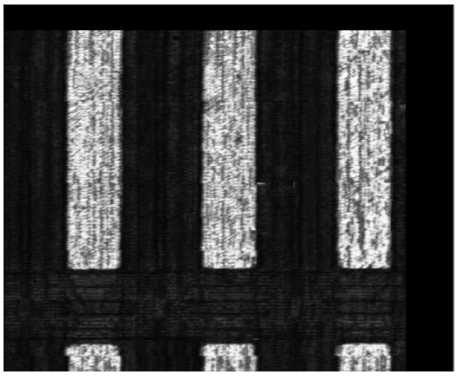

(b) C-scan Post-Impact

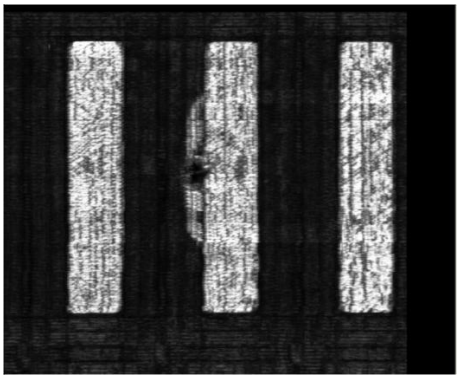

(c) C-scan Post-Static to Limit Load

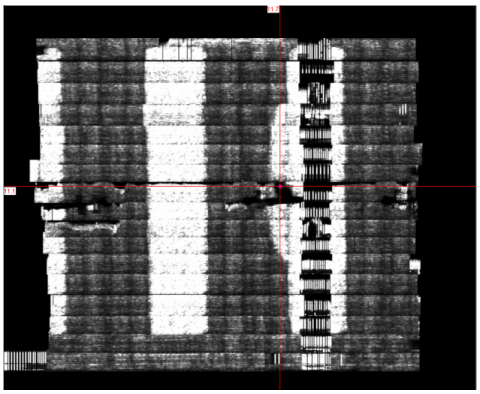

(d) C-scan Post-Cyclic Load

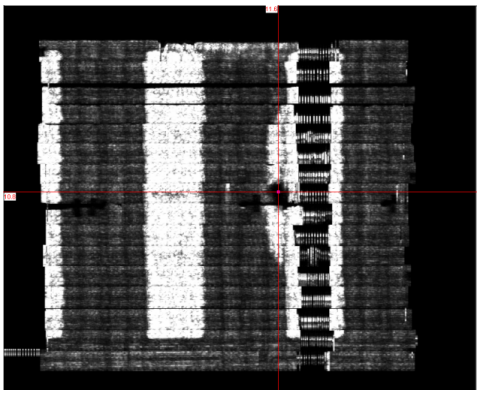

FIGURE 6. C-scans (18”x20”) of the flat 7-stringer panel (a) before and (b) after BVID, (c) after static loading to limit load, and (d) after 20 cycles of compression loading.

2.3.2 Curved 7-Stringer Pressure Panel

Another panel test was performed in collaboration with the Federal Aviation Administration (FAA), utilizing the Full-scale Aircraft Structure Test Evaluation and Research (FASTER) Facility located at the FAA Technical Center in Atlantic City, NJ [14]. This test frame emulated the loads encountered by pressurized aircraft fuselage sections. In this test, a curved PRSEUS panel was subjected to hydrostatic pressure, along with reactive tensile loading at the edges, and axial tensile loads. Phased array ultrasonic testing was periodically employed to monitor a site of BVID near the center of the panel.

Ultrasonic C-scans of the BVID area before and after impact are presented in Fig. 7. There is a considerable amount of artifacts in these scans, caused by difficulty in performing a manual scan within the constraints of the load frame, but these could be distinguished from actual echoes by examining the A-scan waveforms. One such artifact is present in the center of Fig. 7(b). A-scan analysis showed that this area was free from delamination. The scan post-impact is presented in Fig.7(c), and also in Fig. 7(d) with the addition of a cartoon outline to highlight the delamination area. The formed delamination is similar to that observed in the flat compression panel, Fig. 6(c), with an additional small area of delamination between the first two stitch rows.

(a) Curved Panel

(b) C-scan Pre-Impact

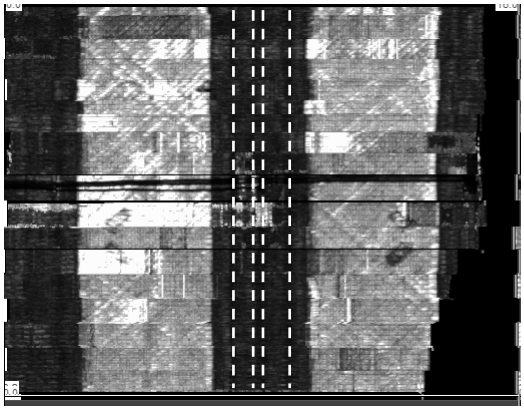

(c) C-scan Post-Impact

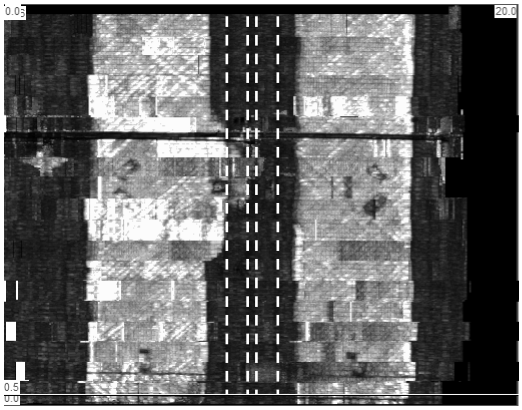

(d) C-scan Post-Impact with Highlight

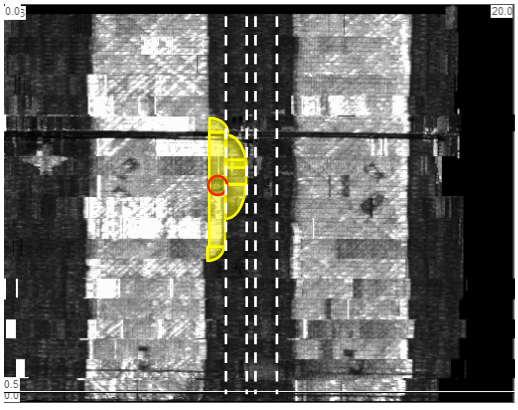

FIGURE 7. (a) Photograph of the curved test panel. (b) C-scan (18”x20”) of panel before BVID. Rectangular indication at center is a signal artifact due to coupling. (c) C-scan of panel after BVID. (d) Post-impact C-scan with a cartoon outline to highlight the delamination and the impact point (circle).

2.3.3 Pressure Cube Test

The final test before the HWB Multi-Bay test was a pressure cube, comprising six flat PRSEUS panels, joined to form a sealed, nearly cubical structure [15, 17-21]. A graphic of the cube is shown in the inset of Fig. 8, with one side removed to show the interior details. The cube test served as a demonstration of the joining concept, planned for the larger HWB Multi-Bay test article. As with the earlier tests, the cube was subjected to BVID, and PAUT inspection identified a minimal amount of damage around the impact site, which remained unchanged throughout the pressure tests. Various stages of pressure were applied, with the final stage being pressurization to failure. Success of the joint test was assured at 18.4 psi pressure, twice the normal operating pressure for an aircraft, but the structure remained intact until 48 psi, when a metallic component of a corner joint began to crack, after which the forward bulkhead panel failed catastrophically. The crown, floor, and other three sides of the cube remained intact, allowing subsequent ultrasonic scans to be performed.

Scans of the remaining panels detected three distinct types of delaminations, distinguished by their locations in the structure. The drawing in Fig. 8 illustrates these three types, labeled A, B, and C. Type A delaminations occur between the laminae of the face sheet, tear or cap strap, and flange layers. The delaminations found in the flat 7-stringer panel and curved 7-stringer panel were of type A. The second delamination type B was observed in the skin or strap layer directly above a perpendicular web component, be it a stiffener, a frame, or an end cap. The final damage type C appeared in the inboard flange layers of end caps adjacent to the interior fillet. Figure 8 includes a B-scan data set of an integral cap to show an example of Type C damage and to illustrate the locations of Type A and Type B delaminations.

A summary of the results for the crown panel is given in Fig. 9. The results for the aft bulkhead and the right and left rib panels are similar in character. The metallic fitting which is believed to have initiated failure was located in the joint at the lower left corner of this figure. This will be referred to as corner I.

In the crown, three areas of Type A delamination were observed, near corner I and along the joint with the failed forward bulkhead. Similarly, on the right rib panel significant areas of Type A damage were along the joint with the forward bulkhead and near corner I. These delaminations were observed to cross stitch rows in places. Because of their location, the Type A delaminations are believed to have formed due to rapid, high intensity load redistribution during the time period between failure initiation in corner I and the final catastrophic failure of the forward bulkhead.

Type B delaminations are observed in Fig. 9 to occur in all of the stringers, extending the entire length between frames, and in the frame ends near each corner. The Type B damage is contained between the central two stitch rows in all of these areas.

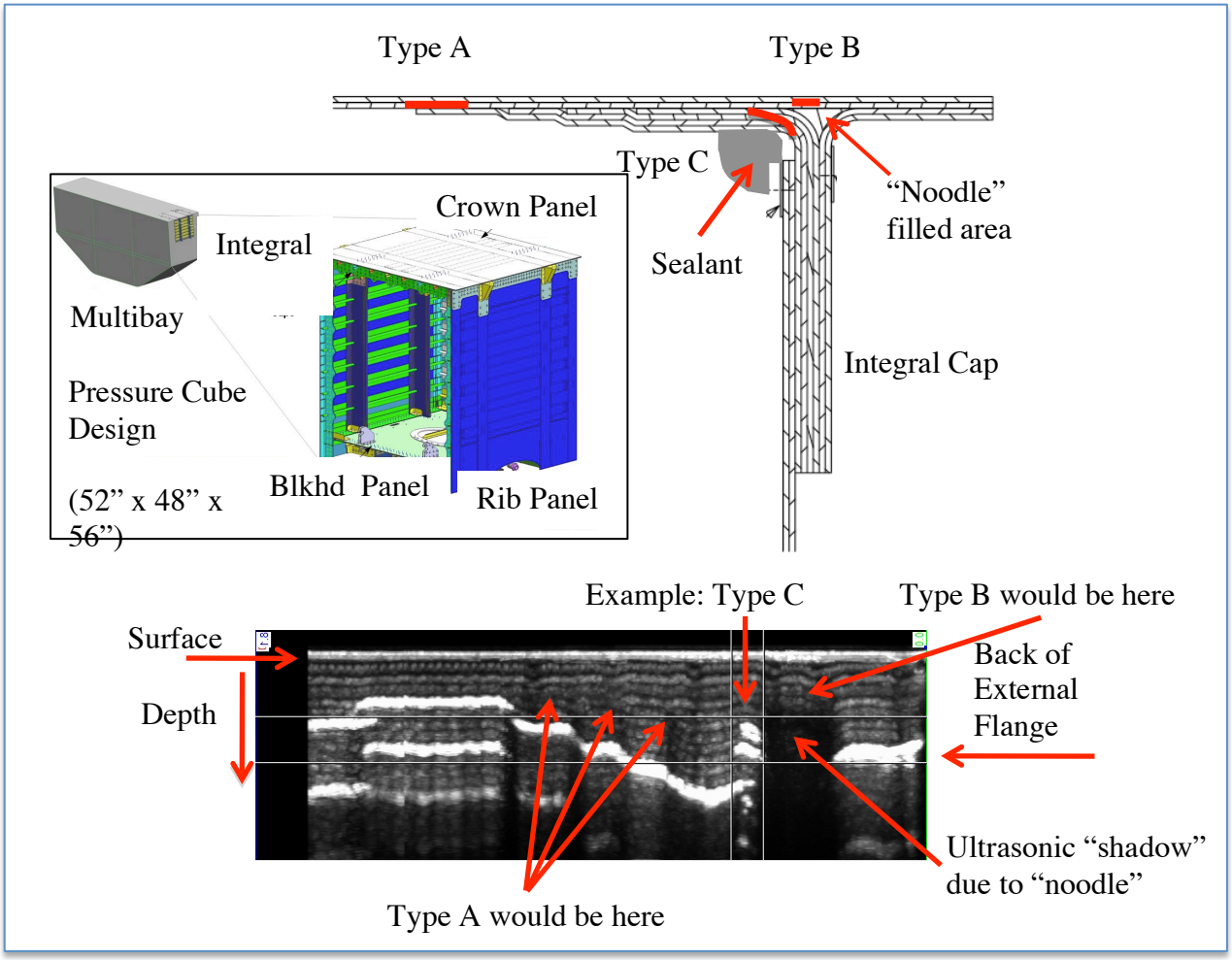

FIGURE 8. The PRSEUS pressure cube (inset) was designed to demonstrate the joint design intended for use on the full large-scale multibay test article. After loading the cube to failure, three types of delaminations were identified, based on location. Type A occurred between face sheet and flange plies; Type B delaminations occurred in the plies above the noodle of reinforcing structures. Type C delaminations occurred in the flange plies adjacent to the inner fillet of the integral cap webs. The fillet region was masked by an ultrasonic "shadow, believed to be caused by the noodle.

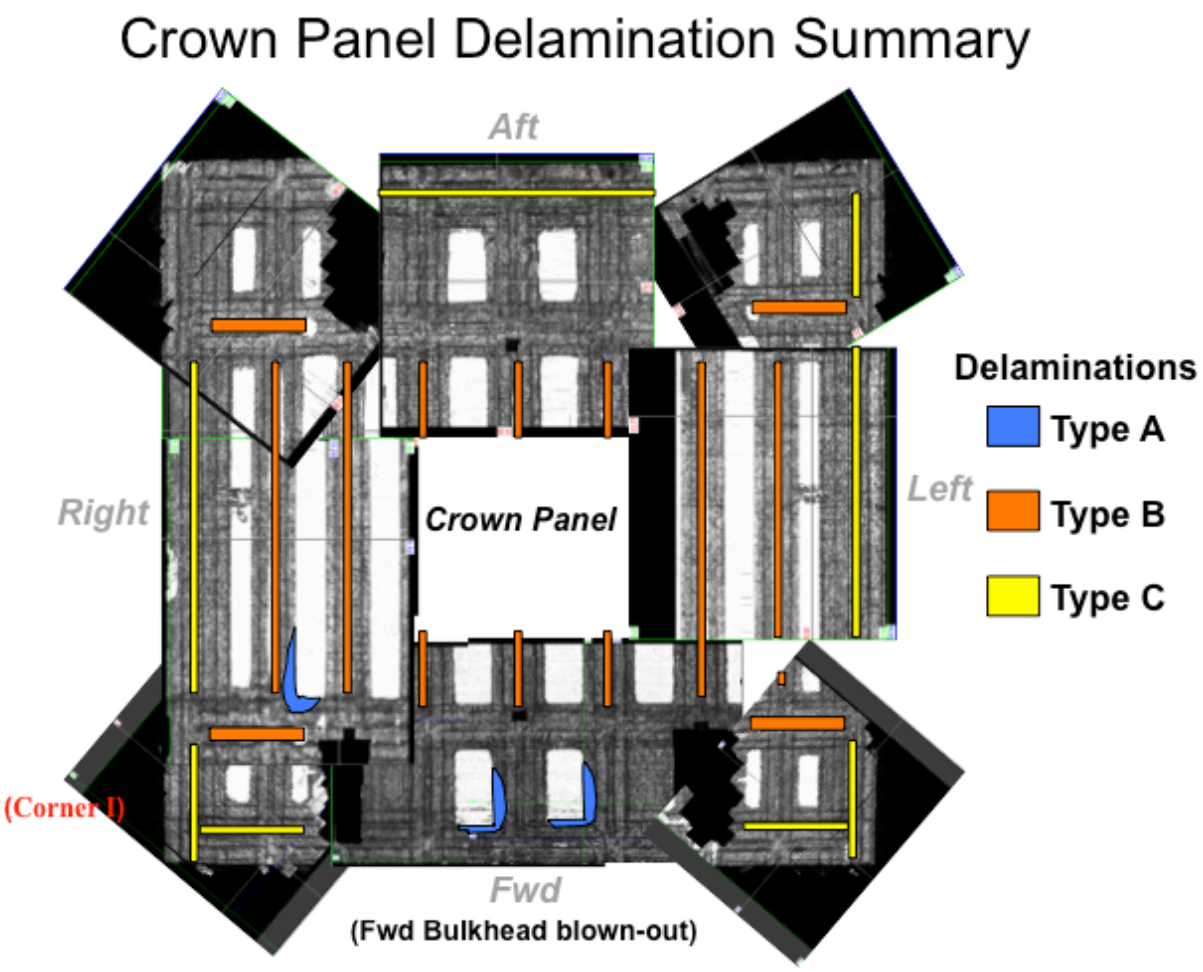

FIGURE 9. A summary mosaic diagram of the delaminations observed in the crown panel of the PRSEUS Pressure Cube after failure. Each rectangular scan approximately 18”x20”.

In the crown panel, Type C delaminations were observed along most of the length of the inner flange of the integral cap. Inboard, the observed Type C flaws did not extend beyond the second stitch row. However, because of the ultrasonic “shadow” above the cap webs (Fig. 8), the extent of these delaminations into the curved fillet was unknown.

In order to address that question, a section of the crown containing an integral cap was excised for immersion UT and x-ray computed tomography (CT). CT images of the fillet region showed that the curved inner fillet was highly delaminated, resembling the layers of an onion. This condition is consistent with the presence of high out-of-plane stresses in the fillet, predicted by analysis, during pressurization. Almost all of these delaminations were seen to terminate at or inside the first stitch encountered, either the diagonal stitch in the face sheet or the normal stitch

in the web. The few delaminations which did pass the first stitch row were observed to end before the next stitch was encountered [17-18].

2.3.4 Rod Push-Out Tests

A parallel study was performed by NASA and Boeing on the structural integrity of the rod-wrap interface, which is critical for maintaining the high strength and bending rigidity of the PRSEUS structure [16]. This study was experimentally based on 0.5-inch long specimens, as depicted in Fig. 10.

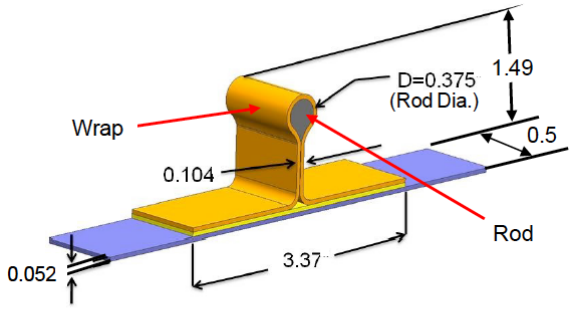

FIGURE 10. Drawing of a typical rod push-out specimen.

A loading device was used to apply axial loads on the embedded rods relative to the overwrap, and the failure loads were measured.

Prior to cutting the as-fabicated stiffeners into short segments, ultrasonic measurements were taken of the rod-wrap interface, as described previously in section 2.2.3, to screen for existing flaws. Examples of the results are presented in Fig. 12. In the upper image, a typical unflawed result is presented. Uniform background ultrasonic scattering is measured from the fiber-matrix interfaces and from the knitting fibers which held the dry stacks together during fabrication.

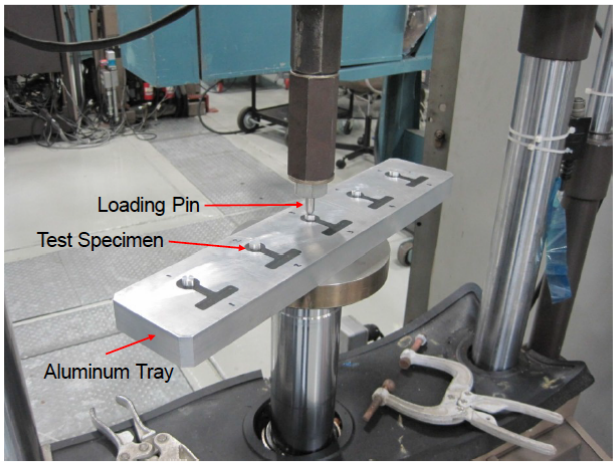

FIGURE 11. Photo of the rod push-out test apparatus.

The middle and bottom images show two examples where existing delamination or extended voiding was observed. By means of these screening ultrasonic scans, specimens were selected for sectioning into short specimens for push-out testing.

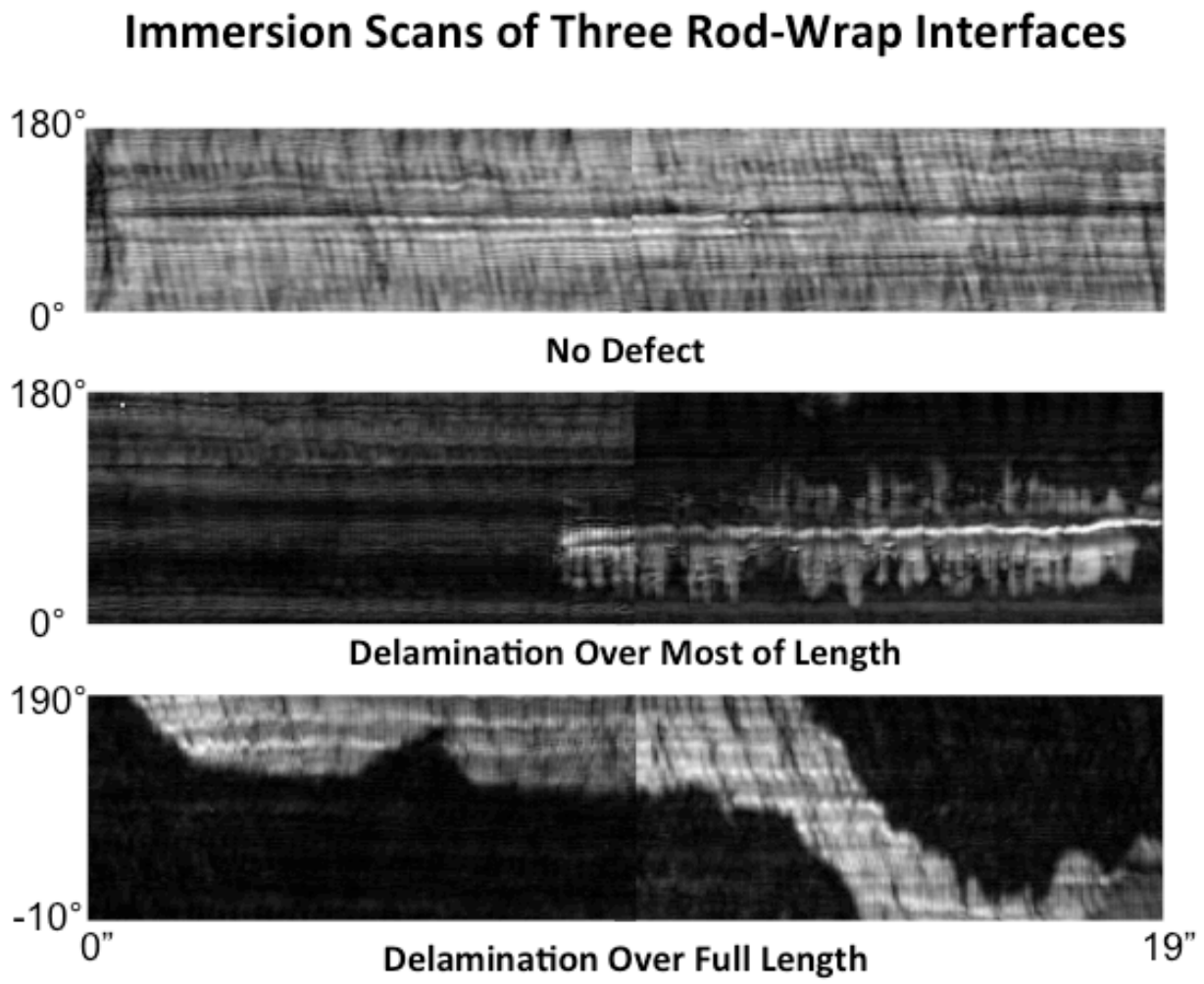

FIGURE 12. Ultrasonic pulse-echo C-scans of three rod specimens prior to cutting into push-out specimens. In the upper scan, the ultrasonic response is relatively uniform, having only normal textural variations resulting from the fabric overwrap. In the center and lower scans, debonds between the overwrap and rod produce echoes much larger than the normal background.

3.0 HWB Multi-Bay Box Test

3.1 HWB Multi-Bay Test Article

The NASA HWB Multi-Bay Test Article was an 80%-scale representation of the center section of the hybrid wing body (HWB) or blended wing body (BWB) airplane pressure cabin (Fig. 13). The 30-ft wide, by 14-ft tall, by 7-ft deep structure was tested using a subset of the critical maneuver and pressure load cases originally used to size the BWB-5-200G baseline configuration. Test results will be used to validate the structural performance and weight predictions used to size the PRSEUS panels that comprise the shell, floor, and bulkhead elements of the baseline airplane.

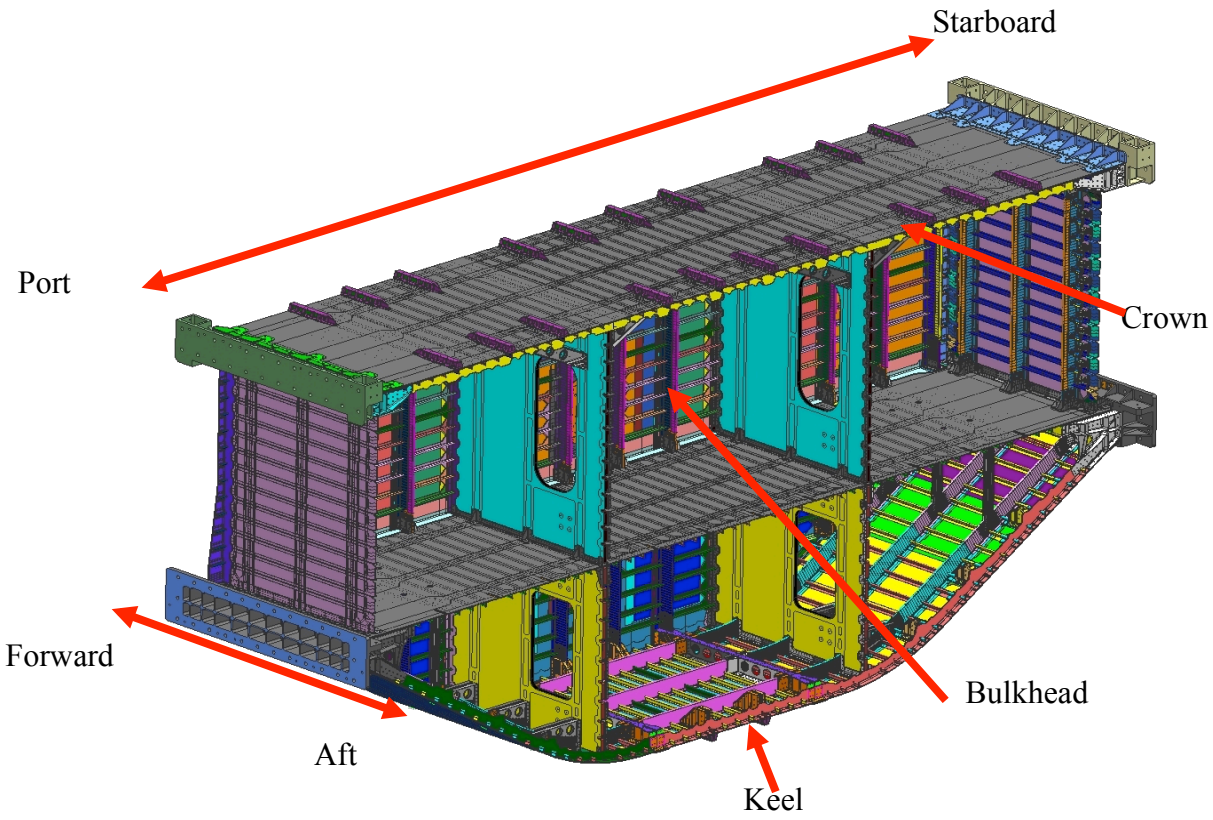

FIGURE 13. A depiction of the HWB Multi-Bay Test Article, with its various parts and directions labeled.

3.2 Multi-Bay Box Test Sequence

The Multi-Bay Box (MBB) underwent pressure and bending load tests at NASA Langley's Combined Loads Test Systems (CoLTS) [22]. A drawing of the MBB test article installed

between the loading platens of CoLTS is presented in Fig. 14. The test article was subjected to internal pressure and external bending loads, individually and in combination. The test sequence was defined in a test specification document [1]. A simplified description of the test sequence as it occurred is given below. Pressure is expressed in terms of 1 sea-level atmosphere (P) and in pounds per square inch (psi). Bending loads are described both in terms of the vertical acceleration simulated in the upward (+) or downward (-) directions in units of gravitational acceleration (G), and in terms of the applied bending loads (top/bottom) in units of thousand-pound force (kip), with compression expressed as positive (+) and tension expressed as negative (-) load. Nondestructive evaluation (NDE) scans were performed as indicated by the bolded text.

- Phase I Checkout
    - -0.5G downbend (-/+ 31.8 kips)
    - 1.25G upbend (+/- 79.5 kips)
    - -0.5G downbend + 0.5P pressure (-/+ 31.8 kips + 4.6 psi)
    - 1.25G upbend + 0.5P pressure (+/- 79.5 kips + 4.6 psi)
- Phase II Design Limit Load (DLL)
    - 1.33P pressure (12.2 psi)
    - -1.0G downbend (-/+ 63.6 kips)
    - -1.0G downbend + 1P pressure (-/+ 63.6 kips + 9.2 psi)
    - 2.5G upbend (+/- 159 kips)
    - 2.5G upbend + 1P pressure (+/- 159 kips + 9.2 psi)
- Phase III Design Ultimate Load (DUL)
    - -1.0G downbend (-/+ 95.4 kips)
    - **NDE**
    - -1.G downbend + 1P pressure (-/+ 95.4 kips + 13.8 psi)
    - 2.5G upbend (+/-238.5 kips)
    - 2.5G upbend + 1P pressure (+/- 238.5 kips + 13.8 psi)
    - 2P pressure (18.4 psi)
- **Pre-impact NDE**
- Perform Impacts
- **Post-impact NDE**
- Phase IV Checkout
    - 0.5P pressure (4.6 psi)
    - -0.5G downbend (-/+ 31.8 kips)
    - 1.25G upbend (+/- 79.5 kips)
    - -0.5G downbend + 0.5P pressure (-/+ 31.8 kips + 4.6 psi)
    - 1.25G upbend + 0.5P pressure (+/- 79.5 kips + 4.6 psi)
- Phase V Design Limit Load (DLL)
    - -1.0G downbend (-/+ 63.6 kips)
    - -1.0G downbend + 1P pressure (-/+ 63.6 kips + 9.2 psi)
    - 1.33P pressure (12.2 psi)
    - 2.5G upbend (+/- 159 kips)
    - 2.5G upbend + 1P pressure (+/- 159 kips + 9.2 psi)

- **NDE**
- Phase VI Design Ultimate Load (DUL)
  - -1.0G downbend (-/+ 95.4 kips)
  - -1.0G downbend + 1P pressure (-/+ 95.4 kips + 13.8 psi)
  - 2P pressure (18.4 psi)
  - 2.5G upbend (+/- 238.5 kips)
- Phase VII Final Failure
  - 3.75G upbend + 1.5P pressure (+/- 238.5 kips + 13.8 psi)
  - 4.125G upbend + 1.5P pressure (+/- 262.4 kips + 13.8 psi)
  - 3.75G upbend + 1.5P pressure (+/- 238.5 kips + 13.8 psi)
  - 3.75G upbend (+/- 238.5 kips)
  - 4.125G upbend (+/- 262.4 kips)
  - Catastrophic failure or 5.0G upbend maximum (+/- 318.1 kips) *(5.0G achieved)*
- **NDE**
- Apply Sawcut to center of crown
- Post-Sawcut Failure
  - Catastrophic failure at 4.25G upbend (+/- 270.3 kips)
- **Post-Failure NDE**

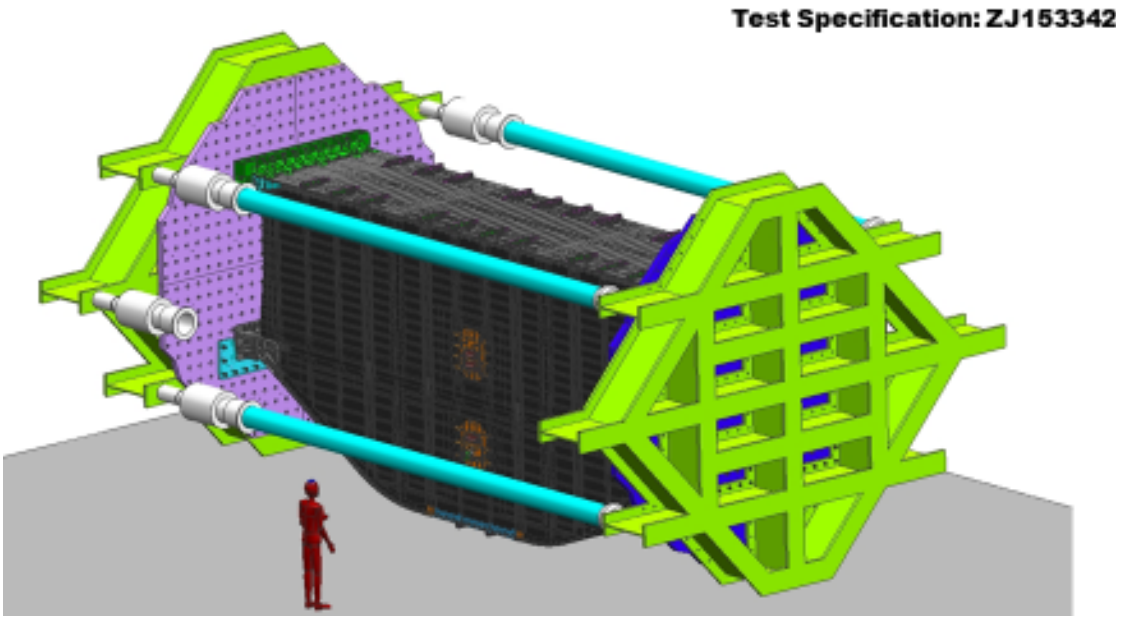

FIGURE 14. Drawing of the Combined Loads Test Systems (CoLTS) with the Multi-Bay Box installed between the loading platens.

3.3 Saw cut and final failure

In Phase VII of the loading sequence, the MBB test article withstood application of the maximum available loads in CoLTS. It was decided to impart discreet site damage on the crown panel to serve as an initiator for ultimate failure of the article. A diamond-shaped opening measuring approximately 24 inches long by 1 inch wide was cut into the near center of the crown through the center frame between stringers S1L and S2L (Fig. 15). A final load sequence was then applied to take the article to failure.

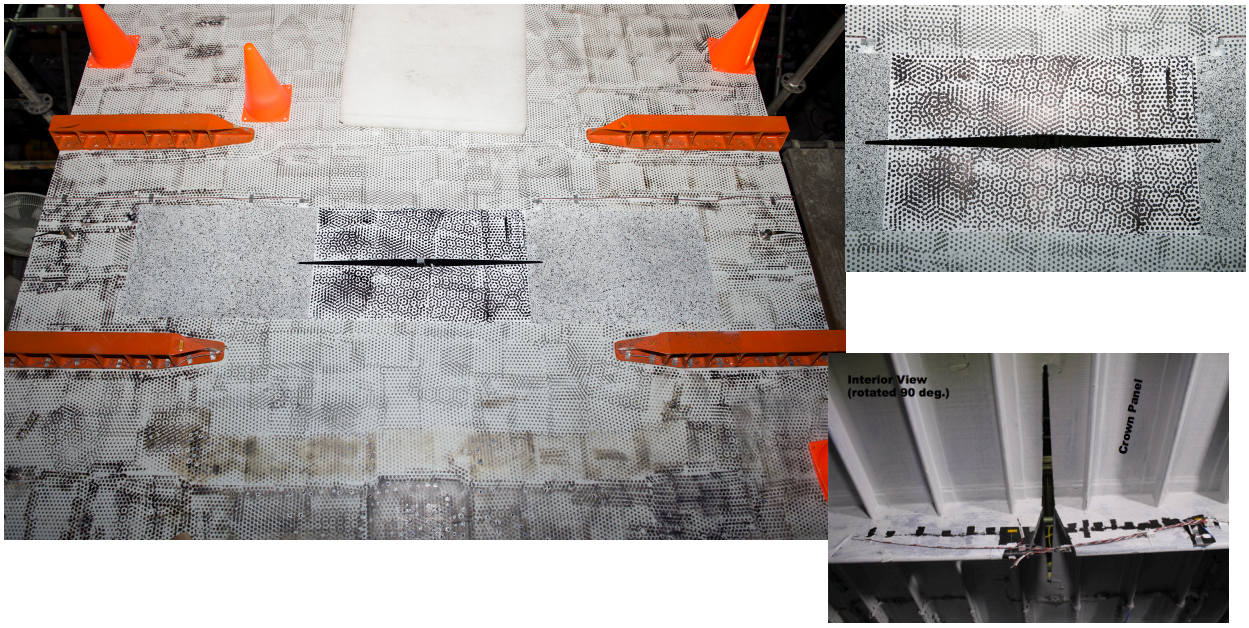

FIGURE 15. Saw cut on the crown of the MBB to initiate final failure event.

3.4 Multi-Bay Box NDE Sites

Six sites were planned to have intentional BVID inflicted as part of the test sequence. During the course of testing, a number of additional sites were identified for NDE. After the final catastrophic failure of the test article, NDE was conducted in several areas surrounding the structural failure crack.

3.4.1 Impact Sites

Three impact sites were located on the center keel panel, with the impacts being performed from the outer skin. The locations of these sites are presented in Figs. 16. Impact #1 was located over the flange of the center frame. Impact #2 was located over the flange of a stringer between the aft frame and the center frame. Impact #3 was located on the skin at the center of a bay between two stringers and between the center frame and the forward frame.

Three additional impacts were located on the forward bulkhead, with impact performed from the inside of the structure. Interior impacts were located as shown in Fig. 17. One interior impact was to the top of a stringer rod. A second impact was positioned on the curved top of a frame. The final impact site was on the skin at the center of a bay between two stringers and two frames.

3.4.2 Sites Identified During the Course of Testing

A number of sites were identified for NDE during the course of testing. The locations of these sites are identified in Figs. 18 and 19.

During the Pressure Cube Test, evidence of Type C delaminations (Fig. 8) was first detected in the interior fillet of the crown end caps during a 2P test. In anticipation that conditions for such delaminations could be produced during the MBB testing, a site was selected for nondestructive monitoring. Figure 18 shows the location on the crown of the site chosen.

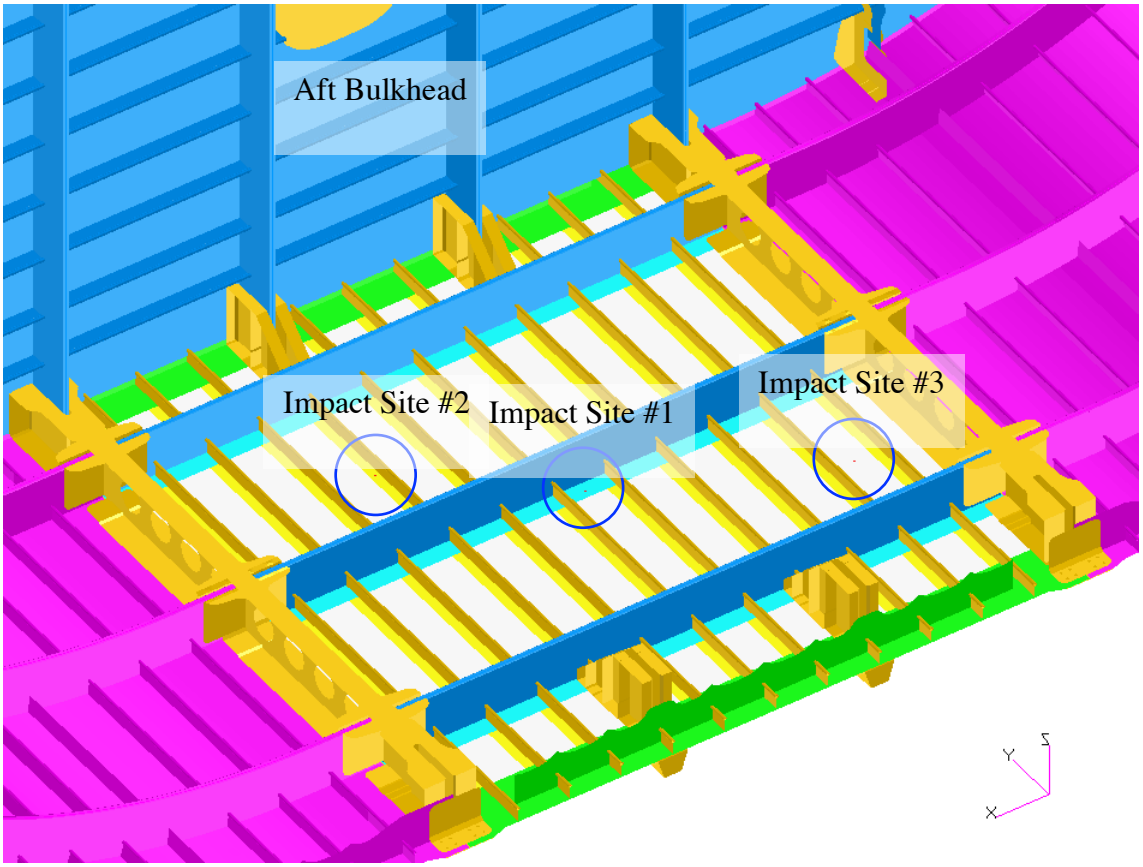

FIGURE 16. Locations of the three impact sites on the center keel of the test article.

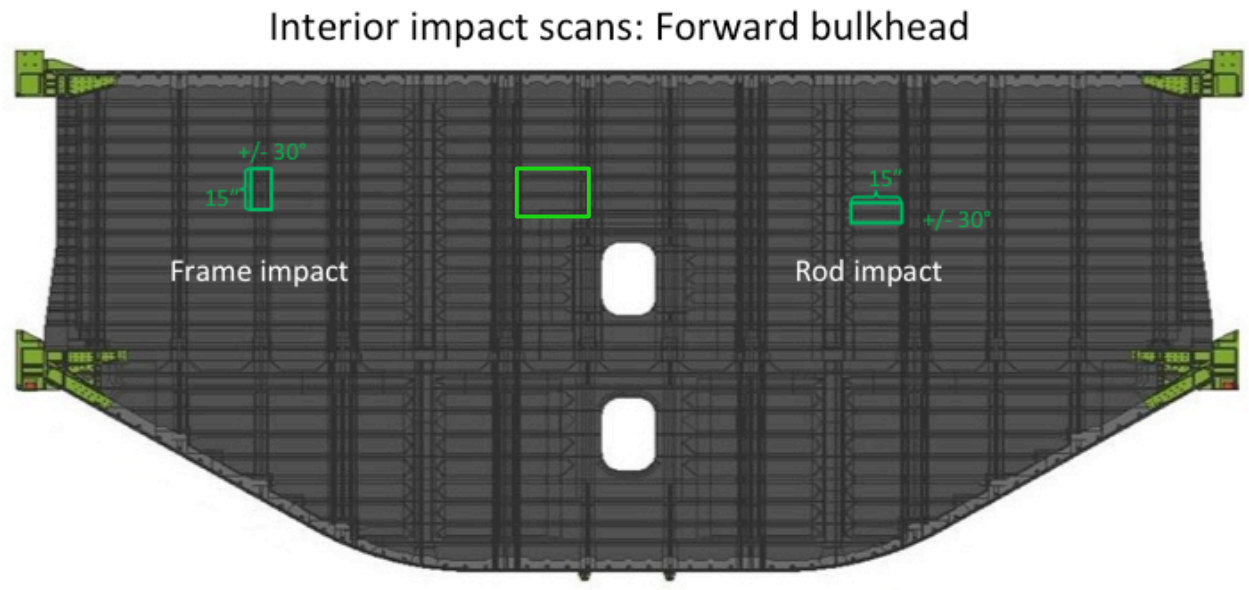

FIGURE 17 Locations of the three forward bulkhead impact sites. These impacts were performed from the inside of the test article. A mid-bay impact was performed just above and to the left of the upper manhole.

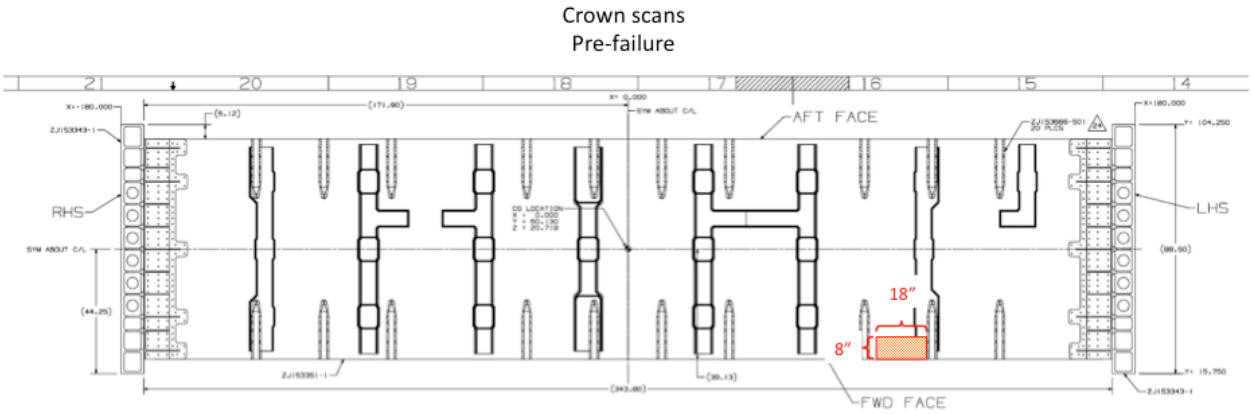

FIGURE 18. Location of the Crown inspection site identified after the Phase III -1.0G load case.

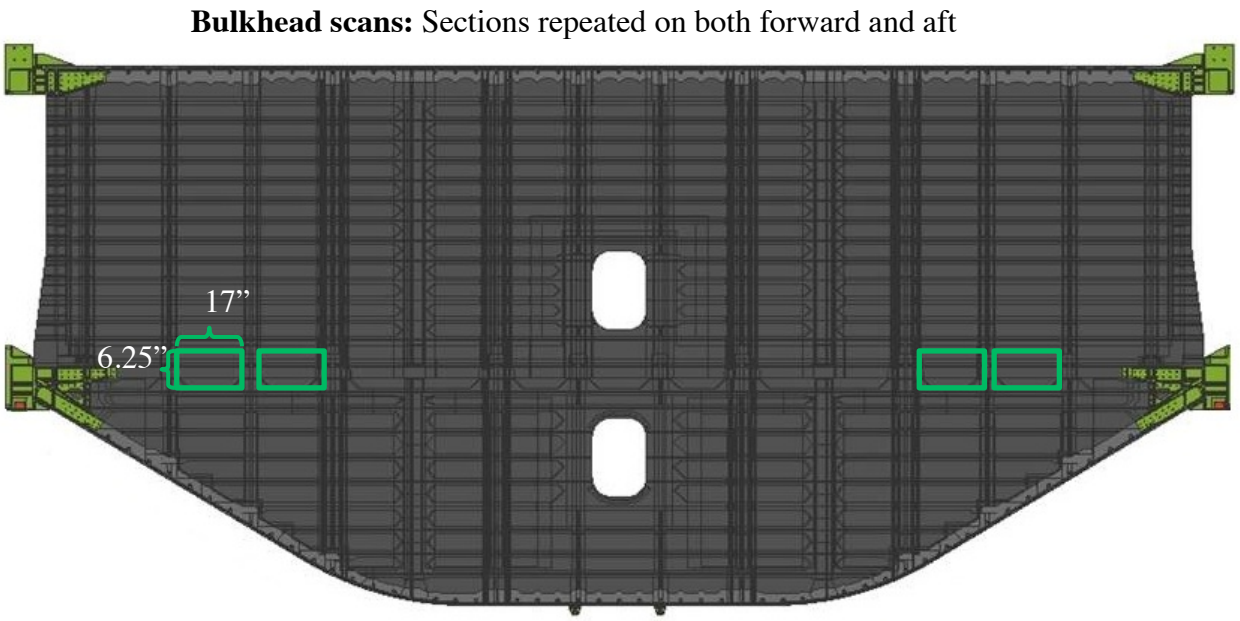

FIGURE 19. Locations of the four forward bulkhead sites identified for inspection following Phase III DUL. Four corresponding sites were also identified on the aft bulkhead.

During the MBB Phase III test, anomolous strain readings near the floor of the upper bay led to identification of eight areas for inspection, symmetrically located on the forward and aft bulkheads. These areas are indicated in Fig. 19.

3.4.3 Sites Identified Following Catastophic Failure

Following the insertion of a sawcut through the central frame of the crown, the MBB was loaded to failure. The failure was manifest in several through-thickness cracks in buckled areas of the structure. NDE was conducted in a number of areas surrounding and adjacent to the failure cracks, as permitted by the physical condition of the structure surface, in order to measure and characterize the damage within the PRSEUS material in the vacinity of the structural failure.

4.0 Ultrasonic NDE Results

Table 1 summarizes the sites scanned, indicating the points during the test sequence that scans were performed. The following sections will address the ultrasonic inspection of different sites chronologically through the post-failure scans.

The detailed structure of the MBB test article is highly varied, such that it is impractical to fully describe the details at each site scanned by ultrasound. However, Figs. 20 and 21 illustrate some key structural features which can aid in understanding the NDE results.

Inspection Location	Time of Inspection During Test Sequence					
	Phase III DUL: following -1G DUL	Pre-Impact	Post-Impact	Post Phase V DLL	Post Phase VII Final Failure Attempt	Post Sawcut Final Failure
Crown	X		X	X	X	X
Frame Impact Site		X	X		X	X
Rod Impact Site		X	X		X	X
Bulkhead Skin Impact Site		X	X	X	X	*
Keel 1: Frame Flange Impact Site		X	X	X	X	X
Keel 2: Stringer Flange Impact Site		X	X	X	X	X
Keel 3: Midbay Skin Impact Site		X	X	X	X	X
Bulkhead Forward Starboard Outer			X	X	X	X
Bulkhead Forward Starboard Inner			X	X	X	X
Bulkhead Forward Port Outer			X			X
Bulkhead Forward Port Inner			X			X
Bulkhead Aft Starboard Outer			X	X	X	X
Bulkhead Aft Starboard Inner			X	X	X	X
Bulkhead Aft Port Outer			X			X
Bulkhead Aft Port Inner			X			
Crown Mid Aft					X	X
Crown Mid Forward						X
Crown Port Forward						X
Crown Starboard Aft						X
Forward Bulkhead						X
Aft Bulkhead						X

* Included in Forward Bulkhead scan below

TABLE 1. Table of inspection sites and points during the test sequence measurements were made.

Figure 20 depicts a cross-section through a typical stringer in the acreage areas of the MBB. The PRSEUS structure is comprised of stacks of fiber plies, which are stitched along the flanges of the stringers. Each stack contains fiber plies of varied orientation, nominally distributed as 44% 0° fibers (parallel to the stringer), 44% ±45° fibers, and 12% 90° fibers, knitted together by non-structural thread.

A cross-section through a frame is presented in Fig. 21. In particular, this figure illustrates the build-up of stacks, which exists in a number of the ultrasonically scanned areas discussed below.

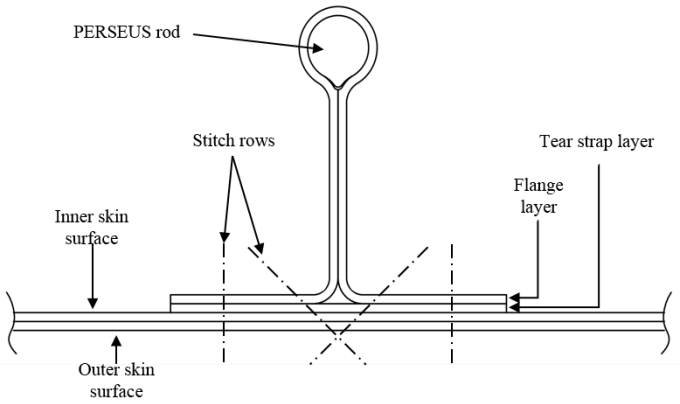

FIGURE 20. Stringer cross section diagram with design terms that will be used in this analysis. Each layer comprises a stack of differently-oriented fiber plies, knitted together. Note that the stitch rows occur in pairs, with one stitch row oriented normal to the fiber stacks, and its partner oriented at 45° to the normal.

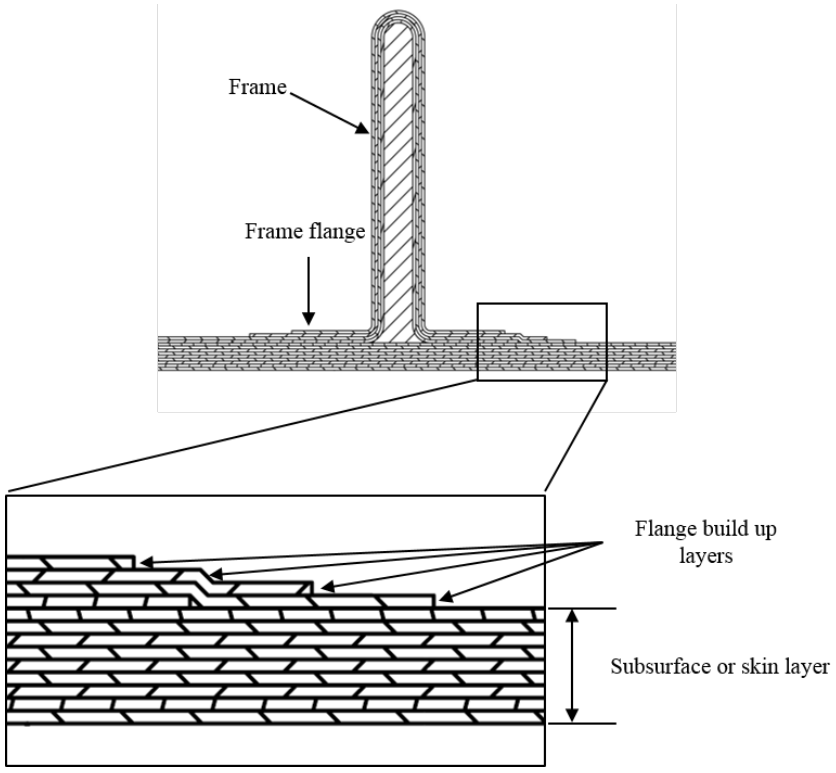

FIGURE 21. Frame cross section diagram with design terms that will be used in this analysis

4.1 HWB Multi-Bay Test Article Impact Sites

As a part of the damage tolerance testing of the MBB test article, several sites were selectively inflicted with BVID. Ultrasonic NDE was performed before and after the impact to quantify the extent of damage produced by the impact. Inspection was also performed at several times during the test sequence to monitor any damage growth between load tests.

4.1.1 Keel Site #1 Over Frame Flange

BVID site #1 on the keel panel of the MBB was located over the flange of the center frame. During the impacting of the frame flange, a positioning error was made in the impacter set-up. As a result, instead of the impacter hitting the frame, as intended, it hit open skin. Since the energy of this impact was set to produce damage in the thicker frame flange, the impacter penetrated the skin (Fig. 22). Because of its penetrating nature, this skin impact resulted in little delamination around the impact site. The delaminations that did occur extended toward the flange areas of the adjacent stringers, but were stopped by the first stitch row (Fig. 23).

The penetration was repaired in order to contain the pressure applied during subsequent testing. The repair was designed to simply contain the pressure, but not carry any skin loads.

Scans performed at various times during the subsequent test sequence, including after catastrophic failure of the test article, indicated no growth in this damage area.

4.1.2 Keel Site #2 Over Stringer Flange

Keel BVID site #2 was located over the flange of a stringer. The impact caused delaminations within the skin layer (Fig. 24A), as well as a delamination at the interface between the skin layer and the stringer flange (Fig. 24B). The delamination within the skin was approximately 2.4 inches along the stringer by 1.1 inches across the stringer. The flange/skin interface delamination was approximately 5 inches along the stringer and 1.3 inches across the stringer. In addition to being contained laterally by the multiple stitch rows in the stringer, an examination of the delamination shows that the flange/skin interface damage along the length of the stringer also appears to stop at the location of an unbroken pair of stitches. Qualitatively, this result is similar to those observed in earlier panel tests (Figs. 6, 7).

Scans performed at various times during the subsequent test sequence, including after catastrophic failure of the test article, indicated no growth in this damage area.

FIGURE 22. Accidental penetrating impact on the keel.

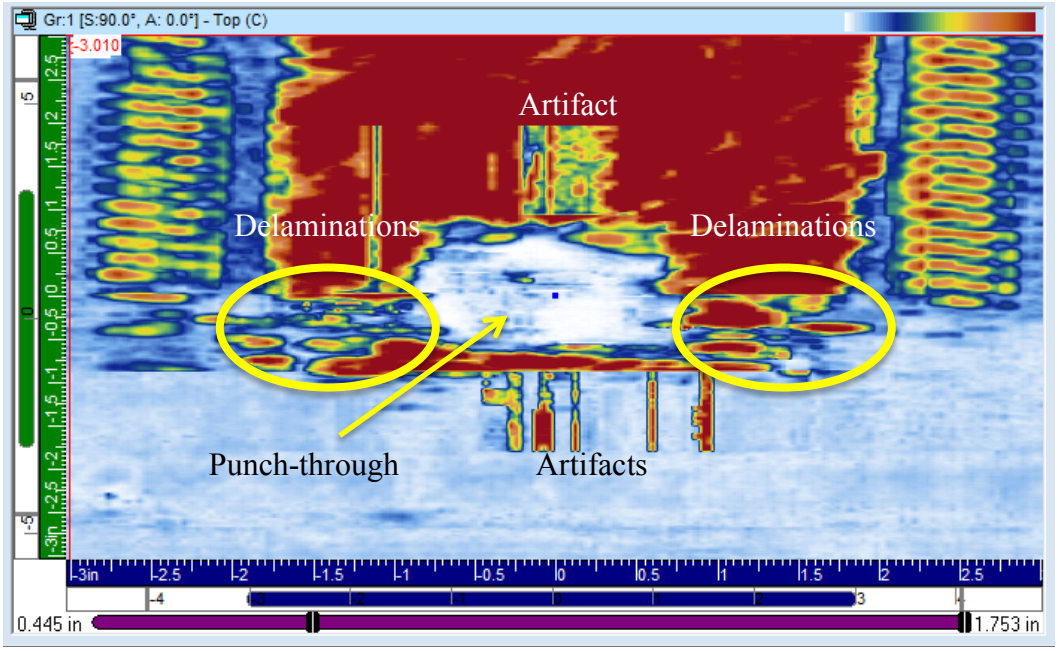

FIGURE 23. Ultrasonic data of the delamination damage caused by the center frame keel impact. Note that the artifacts in this image are a result of strain gage placement which cause an issue in coupling with scanning probe.

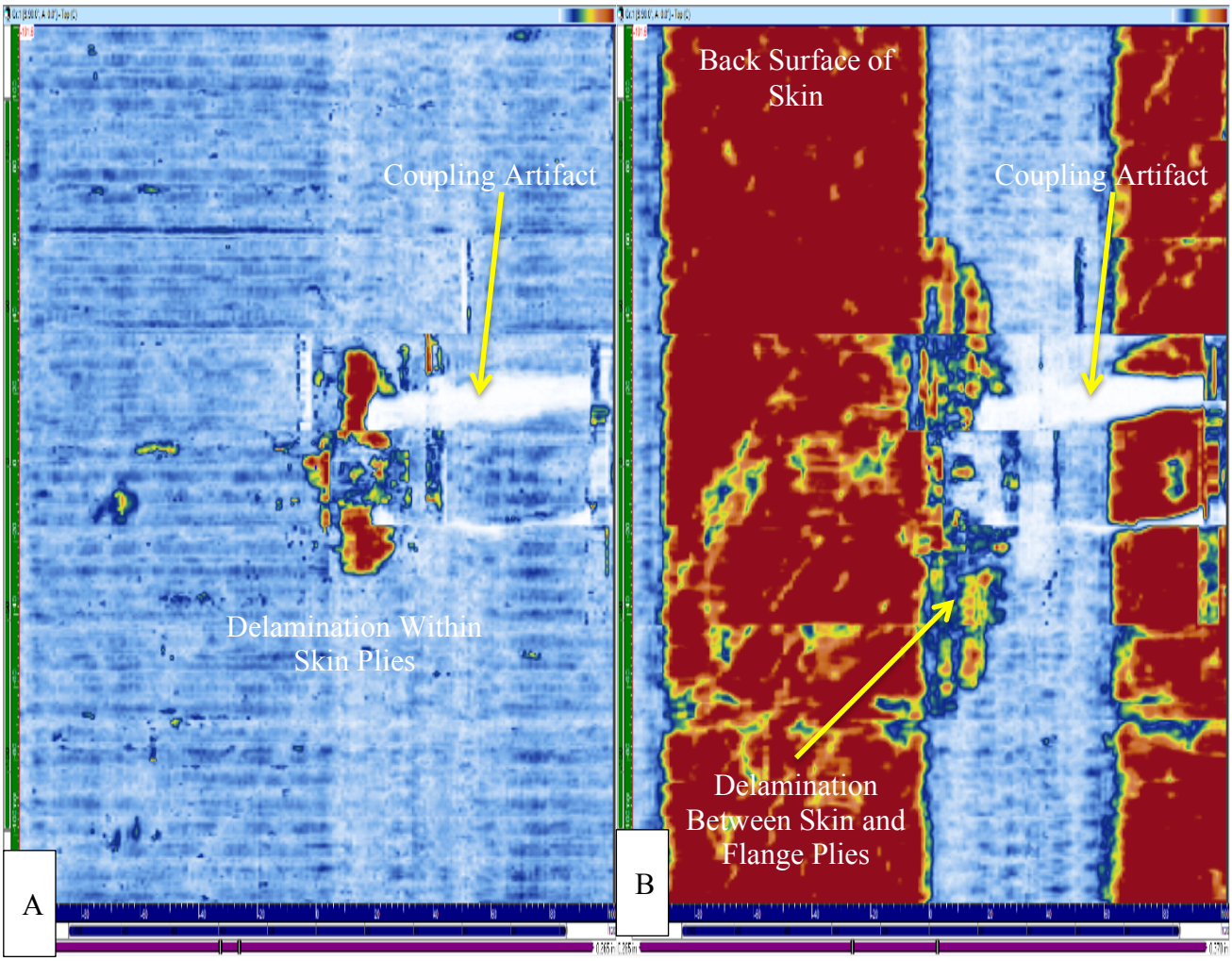

FIGURE 24. Ultrasonic data of the keel impact on the stringer flange. A) delamination in the subsurface/skin layer, B) delamination in the stringer flange/skin layer interface.

4.1.3 Keel Site #3 on Mid-Bay Skin

BVID site #3 on the keel was located on the unsupported skin at the center of a bay, midway between two stringers and two frames. On the inside surface of the skin this impact made delaminations and transverse cracking oriented along the positive 45 degree direction. This

damage stopped at the first stitch line of the stringer flanges on either end (Fig. 25). Beyond some smaller internal skin delaminations surrounding the impact site, this was main damage caused by the impact.

Scans performed at various times during the subsequent test sequence, including after catastrophic failure of the test article, indicated no growth in this damage area.

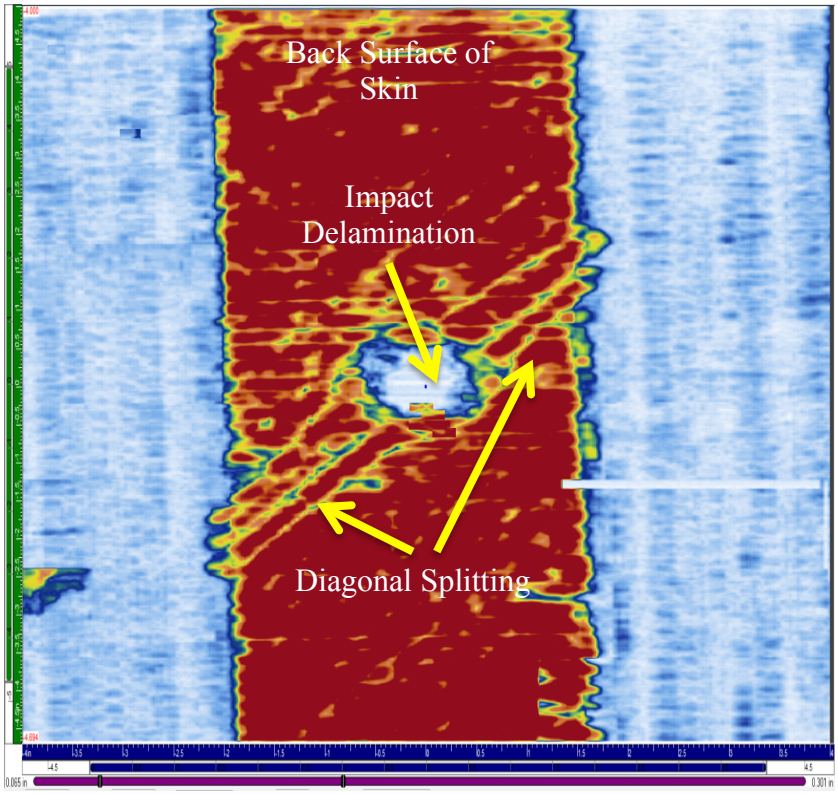

FIGURE 25. Ultrasonic data of the keel impact on the mid bay skin section.

4.1.4 Forward Bulkhead Site in Mid-Bay

On the forward bulkhead, one interior impact site was also located on the unsupported skin at the center of a bay between two frames and two stringers (Fig. 26). Geometrical considerations dictated that the ultrasonic scans be performed from the outer skin surface. The cracked surface, with exposed broken fibers, did not permit the use of the phased array probes, so the site was scanned using a single-element ultrasonic probe and the area of delamination was marked on the surface of the MBB.

The damage was observed to be similar to that resulting from the skin impact on the keel (Fig. 25), with the diagonally-oriented delaminations and associated transverse cracking terminating at the first stinger flange stitch row encounted at each end.

Scans performed at various times during the subsequent test sequence, including after catastrophic failure of the test article, indicated no growth in this damage area.

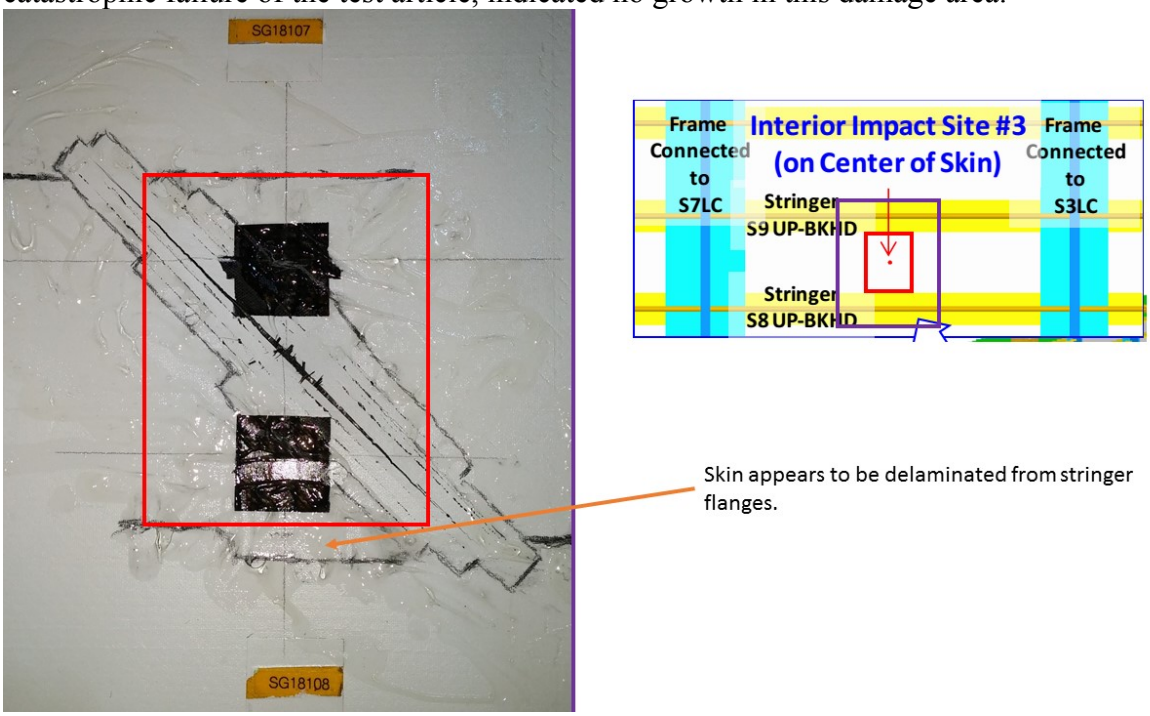

FIGURE 26. Manual ultrasonic scan of forward bulkhead skin impact site. Impact was performed on inner surface of the skin, while ultrasonic inspection were performed from the outer surface of the skin. Delamination and transverse cracking was oriented along a diagonal fiber direction, extending to, and terminating at stringer flanges above and below the impact.

4.1.5 Stringer Rod Impact Site and Frame Impact Site

Both of these impact sites were scanned, using the curved phased array probe, depicted in Fig. 4, before impact and following impact. No indications of damage were observed. These two sites were scanned again, following Phase VII and following failure of the MBB. No indications of damage were found in any of these scans.

4.2 Additional Sites Identified During Load Test

4.2.1 Crown Site

This site was identified as a particularly critical site and a scan was requested following the Phase III, -1G DUL load. The scan showed no indications of delaminations in the fillet of the end cap, or any other flaws or damage. Scans were performed following the completion of Phase III, following Phase V DLL, and following Phase VII, and each of these also showed no damage indications. This location was included in one of the post-failure scans, which will be described. No evidence was observed in this scan of delaminations in the inner fillet of the end cap.

4.2.2 Bulkhead Locations

These sites were called out for scans following Phase III. Scans of all eight areas showed no indications of flaws or damage. Scans were performed on the Aft Starboard Inner and Aft Starboard Outer sites following Phase V DLL and following Phase VII, with no indications found. All of the bulkhead floor sites (except Aft Port Inner) were scanned following failure of the MBB, and no indications were identified.

4.3 Post-Failure Inspection Sites

Results of ultrasonic NDE from a number of areas surrounding the catastrophic failure cracks in the MBB are detailed below: the forward portside section of the crown, which includes the crown area previously scanned; the aft end of the saw-cut on the crown; the buckling crack at the starboard side of the crown; the area around the failure crack on the aft bulkhead; and areas around the failure crack on the forward bulkhead.

4.3.1 Forward Portside Crown

Following catastrophic failure of the MBB, visual inspection of the interior discovered a failure of the forward frame, adjacent to stringer S10LC, the nearest stringer to the left center rib, with some obvious delamination of nearby flanges. Externally, visible signs of damage were limited to some surface bulging, or blistering, above and near the area of the failed frame (Fig. 27).

Post-failure ultrasonic scans were performed from the outer skin over the area identified in Fig. 27. These scans overlapped the area of the crown serially scanned previously to look for inner fillet delaminations in the end cap. As mentioned, no indications of delaminations from the inner fillet were observed.

Figure 28 presents a delamination map for the Forward Portside Crown scans. To produce this map, the ultrasonic echoes were segmented into various times-of-flight (depths) and color-coded areas of observed delamination were superimposed onto the technical drawing of the corresponding location on the MBB. In Fig. 28, an irregular black area indicates the region of

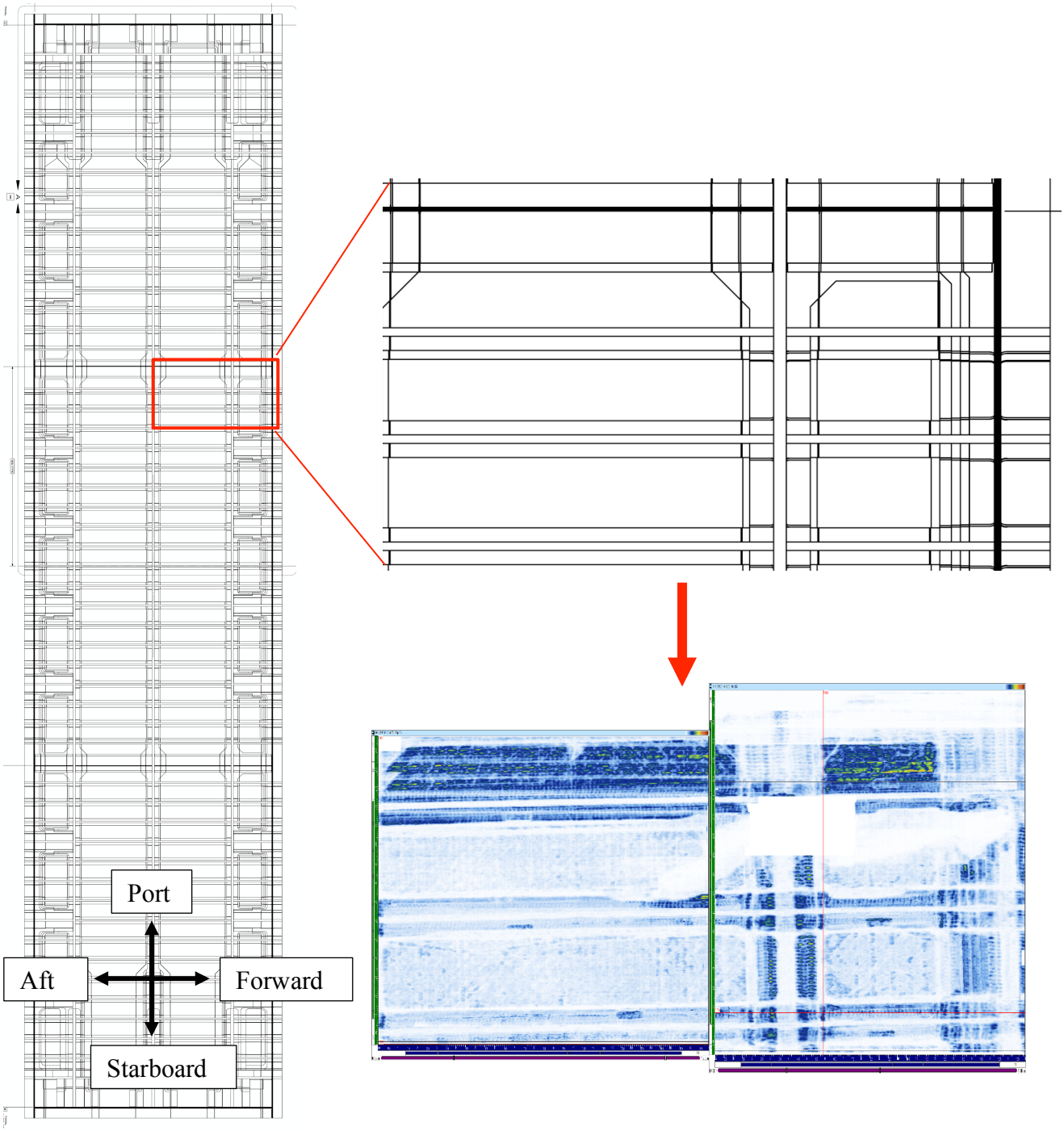

FIGURE 27. The location of the scans performed on the portside forward edge of the crown.

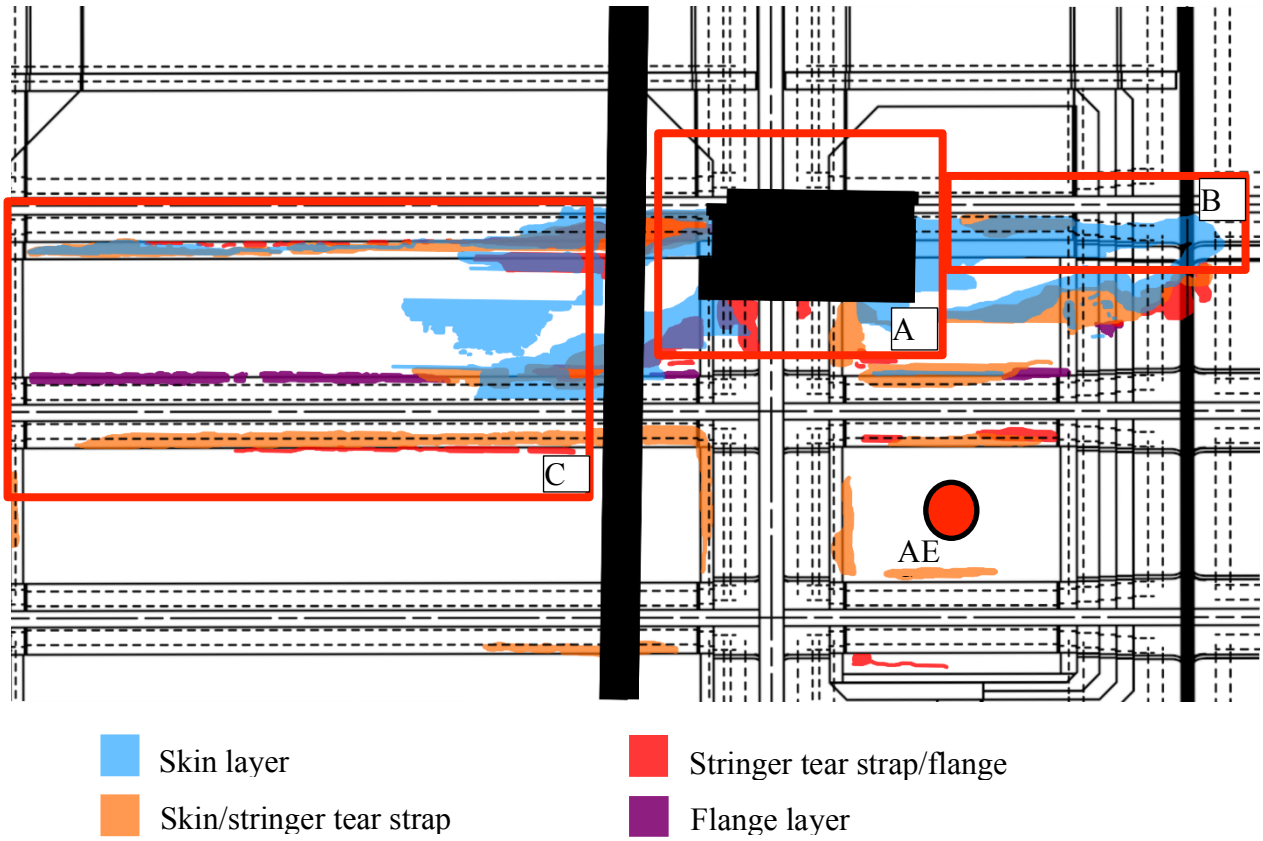

FIGURE 28. (A) Surface damage most apparent when the damage is near an intersection of two built-up areas (stringer and frame). B) Examples of damage contained by stitching. C) Damage growing along the first stich line/skin-stringer interface

surface bulging above the broken forward frame that prevented ultrasonic scanning. A tall, thin black area indicates the gap between the two scanned areas.

The delamination damage in this scan is typical to what is observed in other scans of the MBB, and also bears some similarities and differences to damage observed in previous tests.

One feature which is common to many damaged areas of the MBB is the delamination of the skin stacks in the areas of buckling failure. A concentration of skin delaminations is observed in the skin above the failed frame in this location (Fig. 28A). Over the MBB, this delamination of the skin layers occurs near the most severe damage (e.g., failure crack) in unsupported skin

areas, as well as above stitched flanges and in thickened areas. Where stitches are encountered, the skin delaminations are constrained by stitch rows (Fig. 28B).

Another common feature observed throughout the MBB is the occurrence of delaminations under the tips of flanges (Fig. 28C). This type of delamination is reminiscent of the Type C delaminations observed over the acreage of the Pressure Cube test article (Fig. 9), which occurred between the skin layers and the web of stringers. The differences between these two phenomena are likely because the stringers in the Pressure Cube were undergoing largely tension with some bending, whereas the MBB failure areas were largely in compressional buckling. In both cases, the delamination was contained between rows of stitches.

As pointed out in section 4.2.1 above, the serial scans of the Port Forward Crown site showed no indications of damage through the Phase VII loading. The area which was serially scanned during testing is outlined in green in Fig. 29, while the areas scanned post-failure are outlined in red. Figure 30 shows ultrasonic results in the overlapping area of the green and red areas both before and after the final failure of the MBB. The left-hand panel of Fig. 30 shows the ultrasonic scan following the Phase VII test. The echoes from the inside surface of the doubled skin are well defined, and the interface of these layers with stringers, frame and end cap are clear of delaminations. The right-hand panel of Fig. 30 shows the ultrasonic scan of the same area following catastrophic failure. In this figure it can be seen that flange tip delaminations were not present prior to catastrophic failure, but were observed following the failure. Data measured by a nearby acoustic emission sensor, positioned as shown in Fig. 28, suggests that these delaminations began to occur at approximately 340 seconds before the final catastrophic failure event.

The ultrasonic scan of the area indicated in Fig. 28C also contained an indication that seems to be an out-of-plane wrinkle in the skin layer near one of the stringers. The ultrasonic image is overlaid on the drawing in Fig. 31. The location of this wrinkle nearby a flange tip delamination suggests that it could have contributed to the formation and/or development of the delamination.

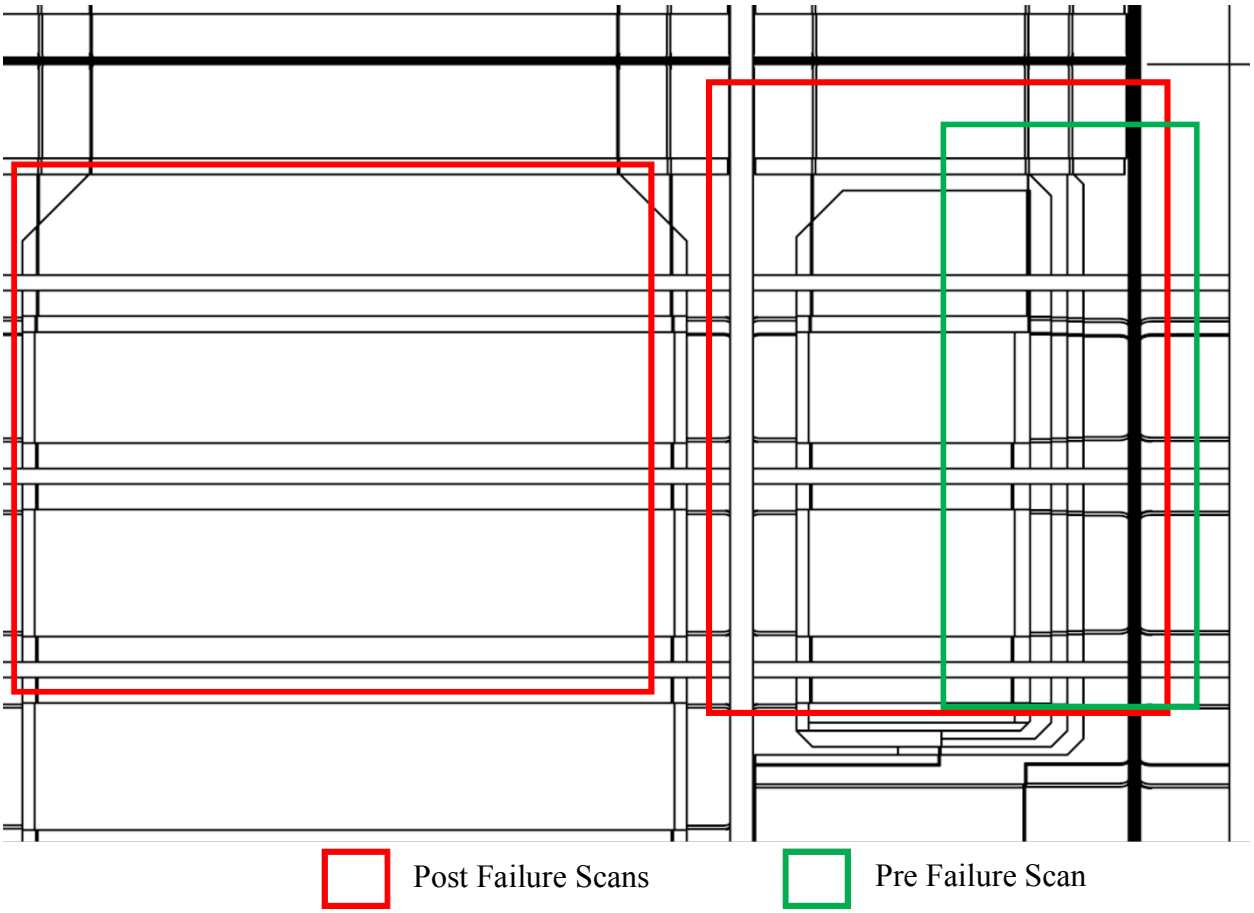

Figure 29. Overlapping sections of the pre and post failure scans on the forward portside crown section.

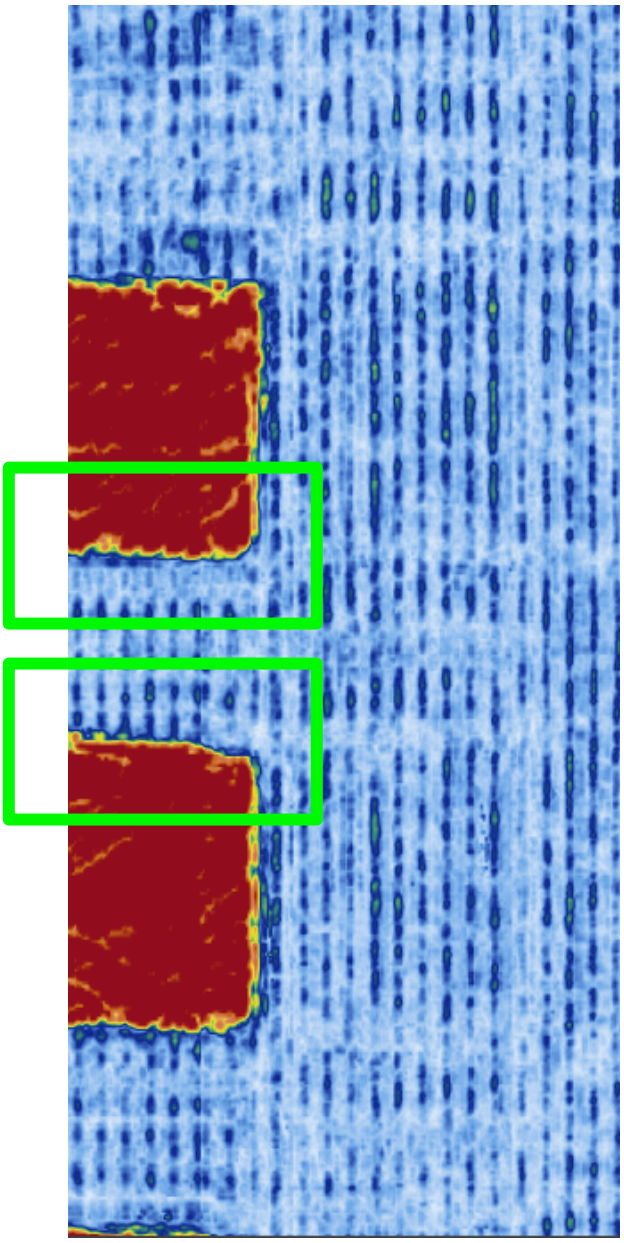

Pre failure scan
(5/12/15 post-DUL test card)

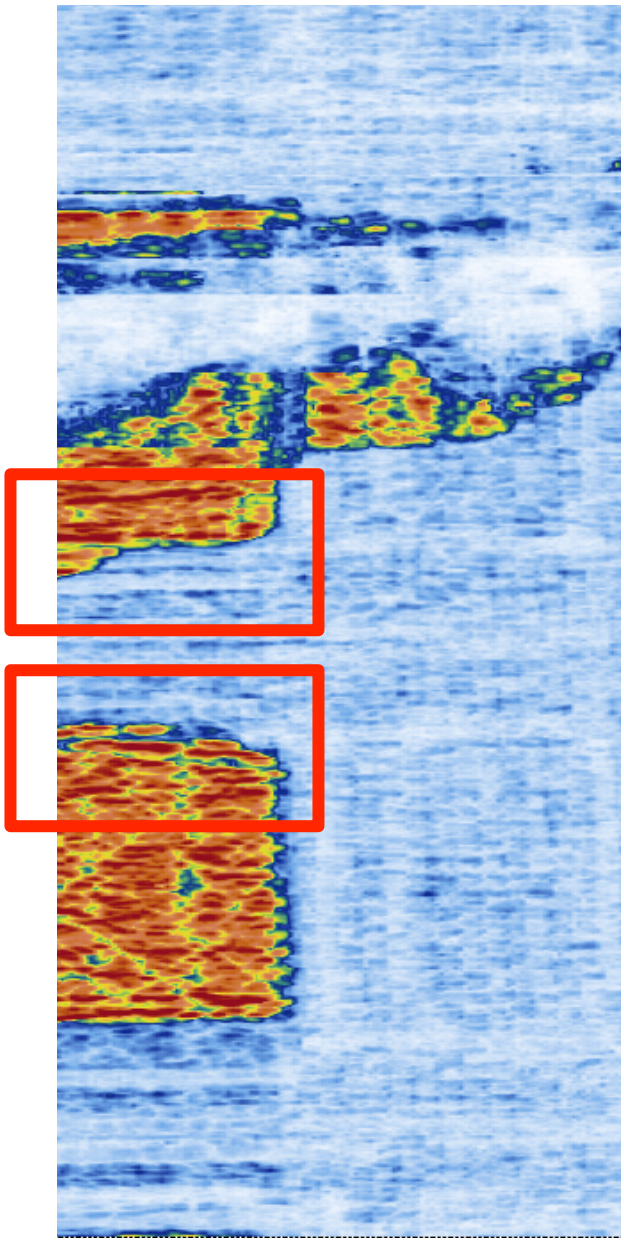

Post failure scan
(6/19/15)

FIGURE 30. Comparison of pre and post fail scans, showing that the damage along the first stitch line of the skin/stringer interface was not present in the scan prior to the failure test. This kind of damage is also seen in all the bulkhead scans and other sections of the crown.

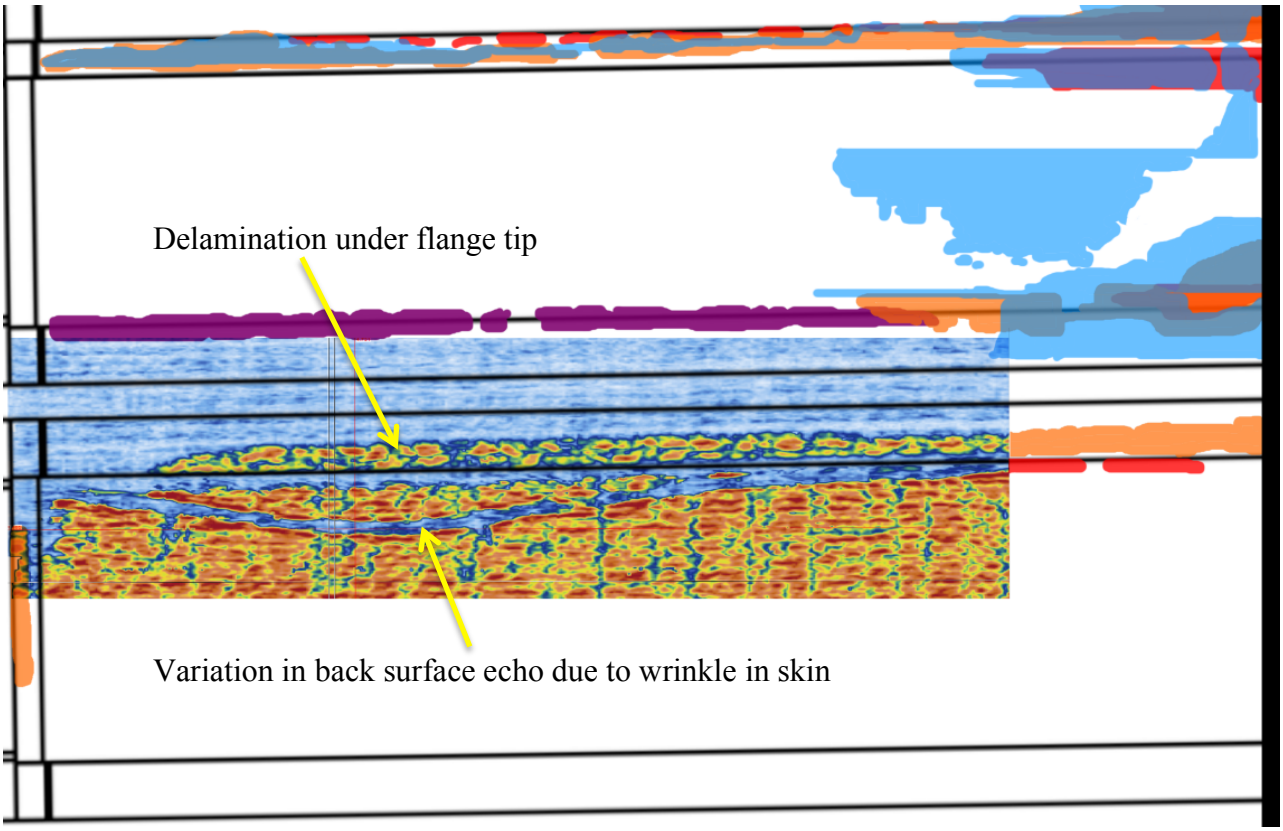

FIGURE 31. Scaled ultrasonic image overlaid with the corresponding technical drawing to show the presence of a skin layer wrinkle, which is also close in proximity to a first stitch line stringer/skin layer interface delamination.

4.3.2 Aft Mid Crown

Figure 32 shows the area scanned surrounding the failure crack initiating from the aft edge of the saw cut. Visual inspection of this area shows the crack extended under the aft frame, resulting in compression failure of the aft frame above stringer S1C. Surface buckling/delamination was observed to extend part of the distance between the broken aft frame and the aft tee cap.

A map of ultrasonic indications in this area is presented in Fig. 33, with color-coded areas of delamination superimposed on a technical drawing of the structure. The area containing the failure crack and other areas containing surface irregularities or acoustic emission sensors, that prevented scanning, are shown in black.

Delaminations within the skin and between the skin and doublers are observed surrounding the failure crack, and these are seen to be contained between the adjacent stringer stitches. These delaminations extend further aft than are apparent from visual inspection of the outer surface, however the delaminations do not pass further aft than the stitch rows of the aft tee cap.

In this region, flange tip delaminations occurred between the stringer flange and skin interface contained by stitch lines (Fig 33A, 33C), as observed in the forward portside crown scans. A deeper delamination was observed above the web of the failed frame (Fig. 33B). An area of delamination is observed in the skin of the bay lying between the aft frame and aft tee cap, and between stringers S1C and S2RC (Fig 33C), which terminates at the crossing of stringer S2RC with the aft tee cap.

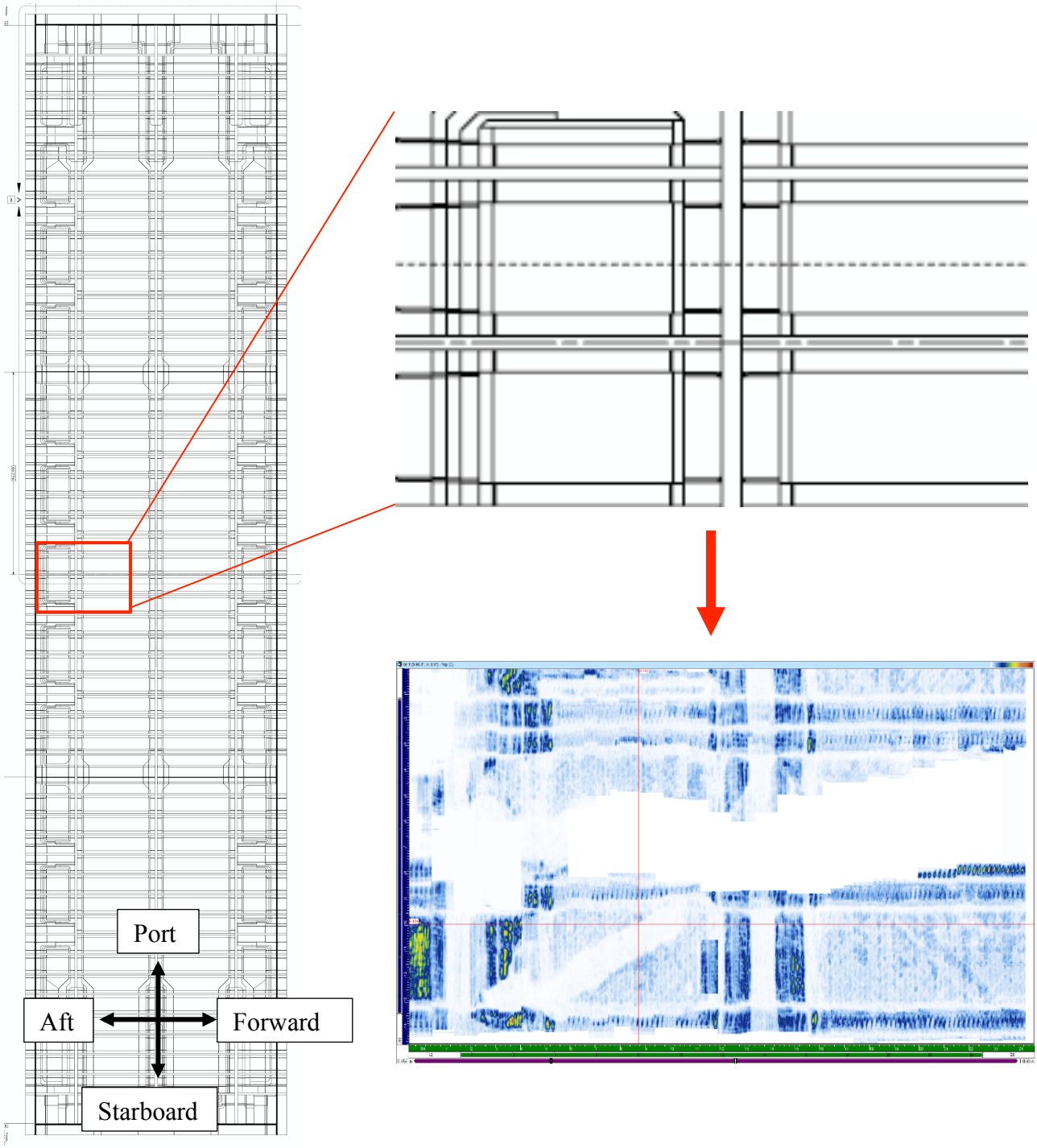

FIGURE 32. The location of the scan performed on the aft side of the saw cut.

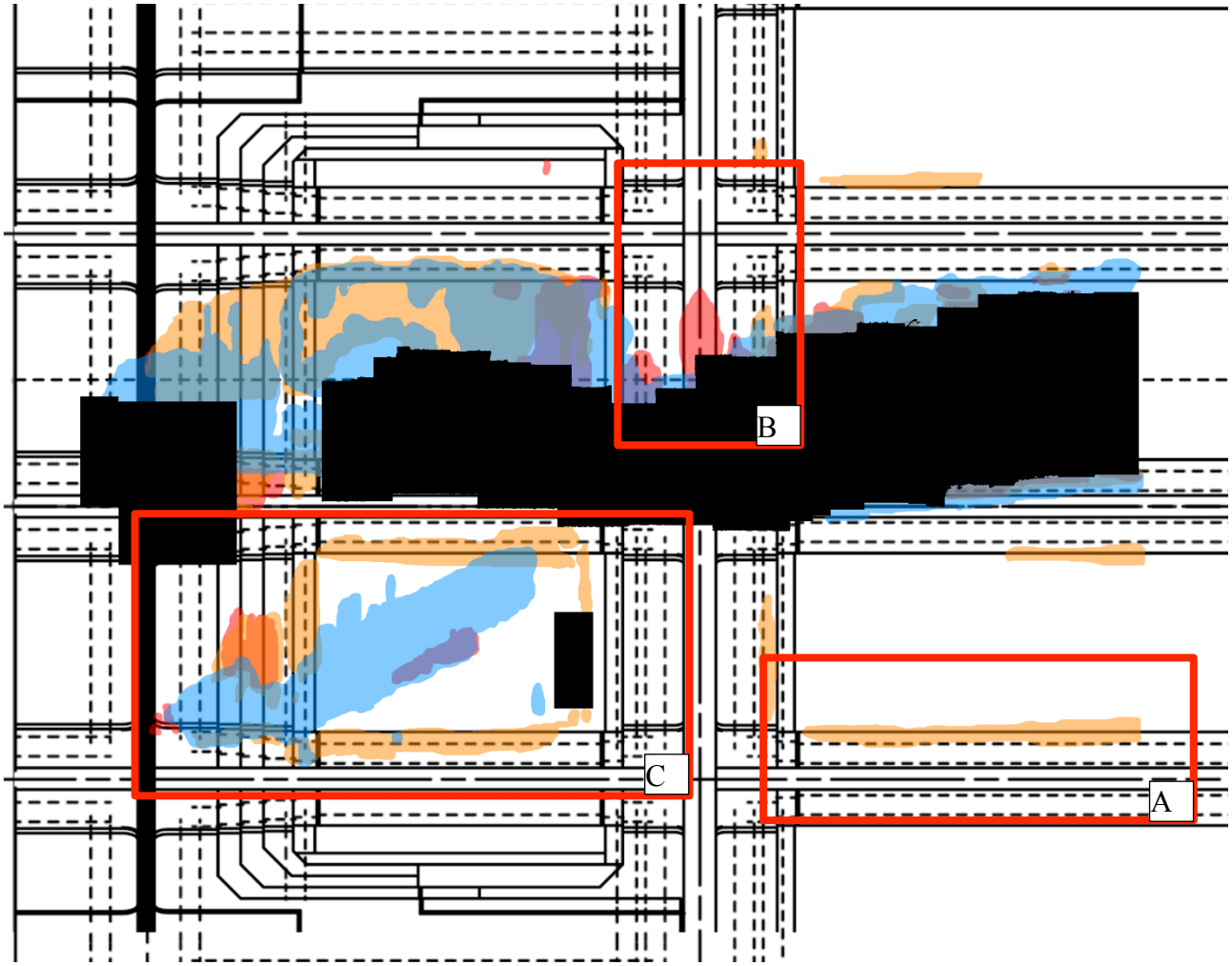

FIGURE 33. A) Delaminations between the stringer tear strap and skin interface along the first stitch line. B) Deep delaminations along the underside of the frame itself. C) Delaminations that extend beyond the stringer and into another skin bay.

4.3.3 Aft Starboard Crown

Figure 34 indicates the location of the ultrasonic scan performed around the buckling crack on the aft starboard side of the crown, near the right center rib. Visual inspection of the interior of the MBB showed failures of the center frame and the aft tee cap at their intersections with stringer S9RC, and failure of the aft frame at its intersection with stringer S8RC. These were connected by a skin buckling crack which continued past the failed tee cap into the aft bulkhead panel.

A delamination map is presented in Fig. 35. The area containing and immediately adjacent to the failure crack was raised and prevented ultrasonic scanning, and is delineated as solid black. Areas of delamination occurring within the skin layers are shown as blue and those occurring between the skin layers and the tear strap layer are shown as orange. Very little delamination damage was observed outside the immediate vicinity of the failure crack, and that was contained by stitch rows.

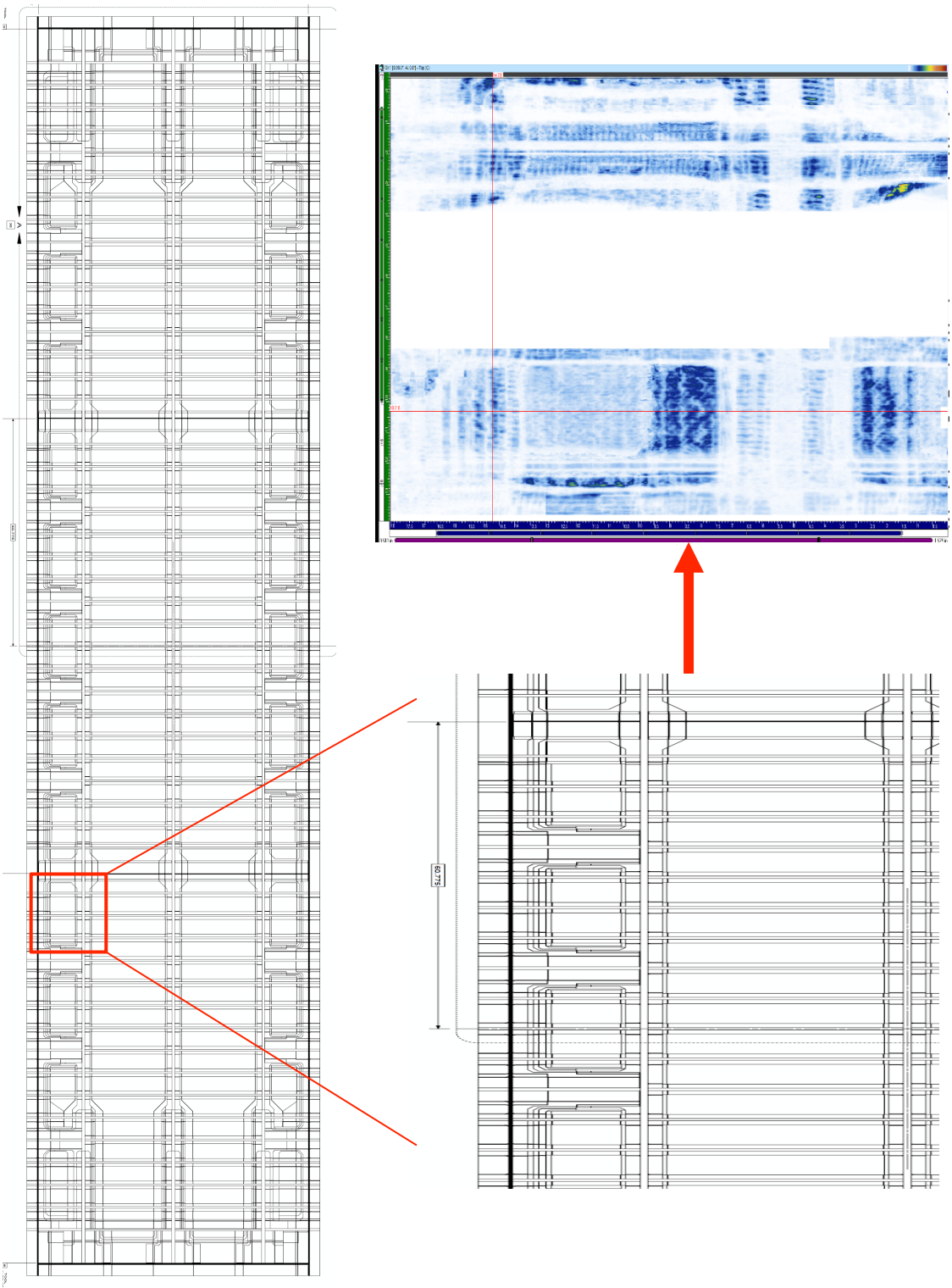

FIGURE 34. The location of the aft edge scan of the starboard failure crack.

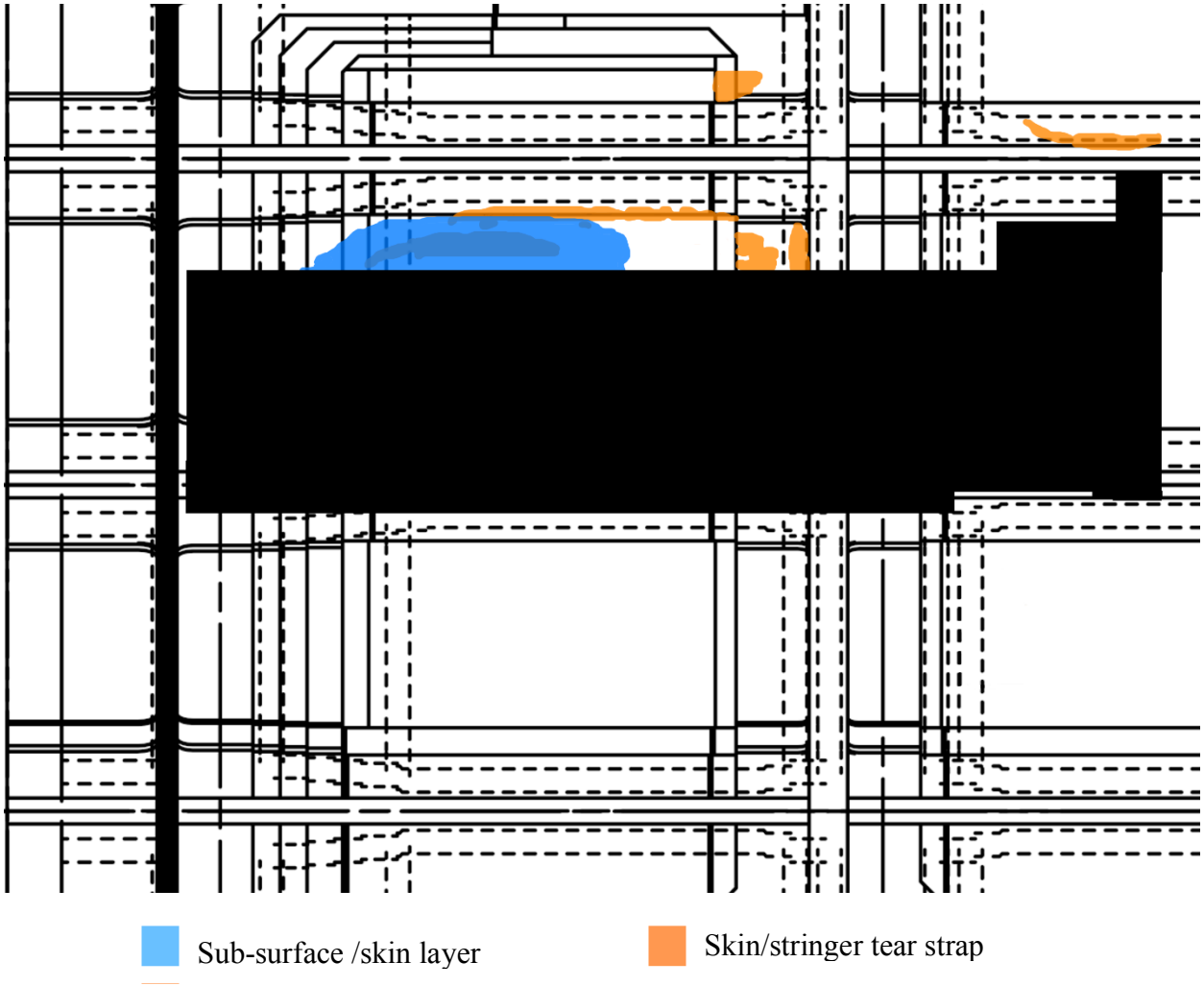

FIGURE 35. Damage map showing the delaminations surrounding the aft end of the starboard failure crack on the crown.

4.3.4 Forward Bulkhead

Figure 36 presents photographs of the exterior of the MBB showing the failure crack, forward of the crown saw cut. Visual inspection of the exterior and interior of the MBB showed that the crack ran through the crown skin between the saw cut to the forward frame. The forward frame was found to have failed at that point. The crack is observed to pass diagonally forward from the failed frame, joggling across stringer S1C (stringer 1, crown) to the intersection of stringer S2RC (stringer 2, right side of crown) with the forward tee cap (Fig. 35A). The tee cap is observed to have failed through the keyhole cutout and downward into the forward bulkhead skin (Fig. 36C).

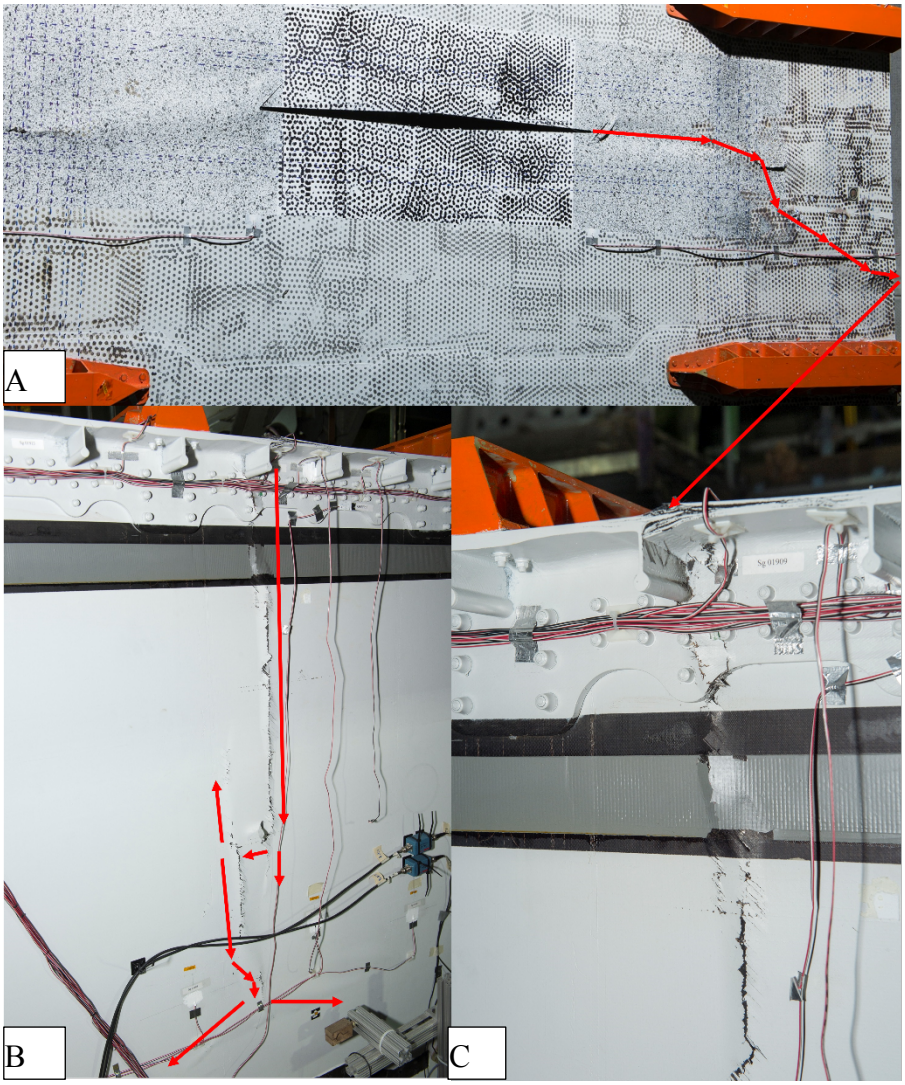

FIGURE 36. Photos of the failure crack that started from the forward side of the crown and extends into the forward bulkhead.

In the forward bulkhead skin, three vertically-oriented buckling cracks are observed, with one horizontal connecting crack (Fig. 36B). One vertical crack runs from the failed upper tee cap, down to stringer S9 UP-BKHD (stringer 9, upper bulkhead). Compression failures are observed in the stringer rods of both S13 UP-BKHD and S12 UP-BKHD where the skin crack intersects them. A second vertical crack is observed between stringers S8 UP-BKHD and S11 UP-BKHD, along the edge of the frame tear strap. Compression failure of the stringer rods is observed in stringers S9 UP-BKHD, S10 UP-BKHD, and S11 UP-BKHD. A horizontal crack is observed along stringer S10 UP-BKHD, connecting these two vertical cracks. A third vertical crack is

visually observed from inside the MBB between stringers S8 UP-BKHD and S7 UP-BKHD, with a rod compression failure in S8 UP-BKHD.

Phased array inspection of the failed area of the crown forward of the saw cut was hampered by poor coupling of the probe to the severely blistered (obviously delaminated) and broken skin surface. Ultimately, a mechanical failure of the probe housing rendered the probe unusable. A replacement was not readily available, so usable scans of this area were not obtained.

Six overlapping ultrasonic scans of the forward bulkhead around the visible cracks were performed. The location and outline of the extent of these overlapping scans on the upper bulkhead is presented in Fig. 37. Figure 38 presents a compilation of the delaminations detected in this area.

Figure 39 is an enlarged view of the upper portion of the scanned area. In Fig. 39A, a large horizontal delamination running parallel to the stringers is seen at the intersection of the crack and the 2nd stringer. These delaminations were mostly contained to within the first or second stitch line of the stringer, and only occasionally extend beyond the top flange but never through the bottom flange. Between the 2nd and 3rd stringers there are horizontal delaminations extending into the flange buildup area of the nearest frame (Fig. 39B). At first glance it would seem these delaminations extended freely into the frame build up without regard to stitching, but upon examination of the details of the stitching in this area it is seen that this is not the case. Figure Fig. 40 that some of the stitching call-outs were not stitches that ran perpendicular to the surface, but were rather stitched at a 45 degree angle to the surface. The technical drawing in Fig. 39 only shows where the stitch exits on the inside of the bulkhead, so when this is taken into consideration the delamination clearly stops at a 45 degree stitch line past the center of the frame.

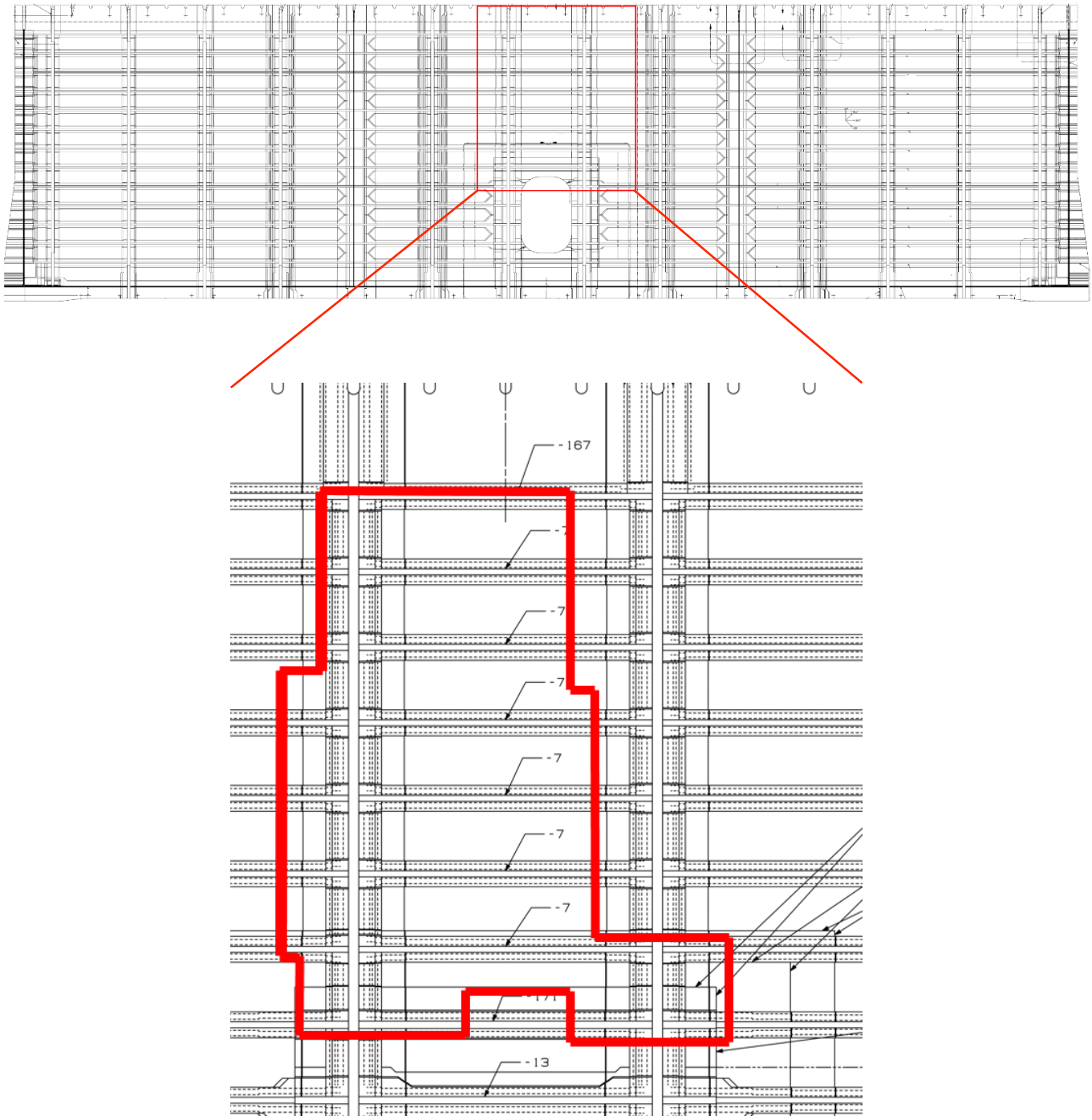

FIGURE 37. The location of the six forward bulkhead scans

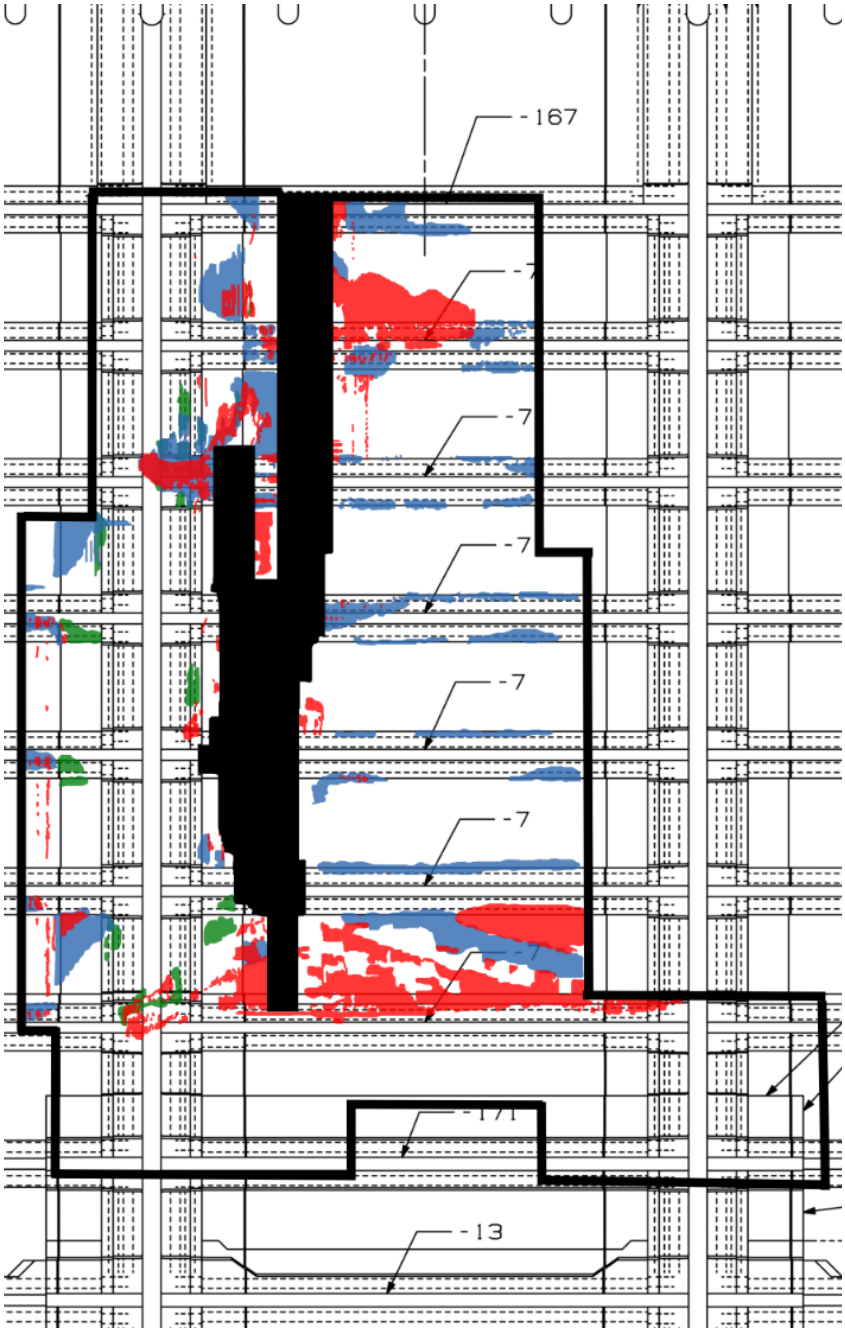

FIGURE 38. A compilation of the delamination damage from the six scans surrounding the failure crack, with the delaminations separated into three different depth locations. Areas containing cracks were too badly damaged to permit ultrasonic coupling, and are indicated in solid black.

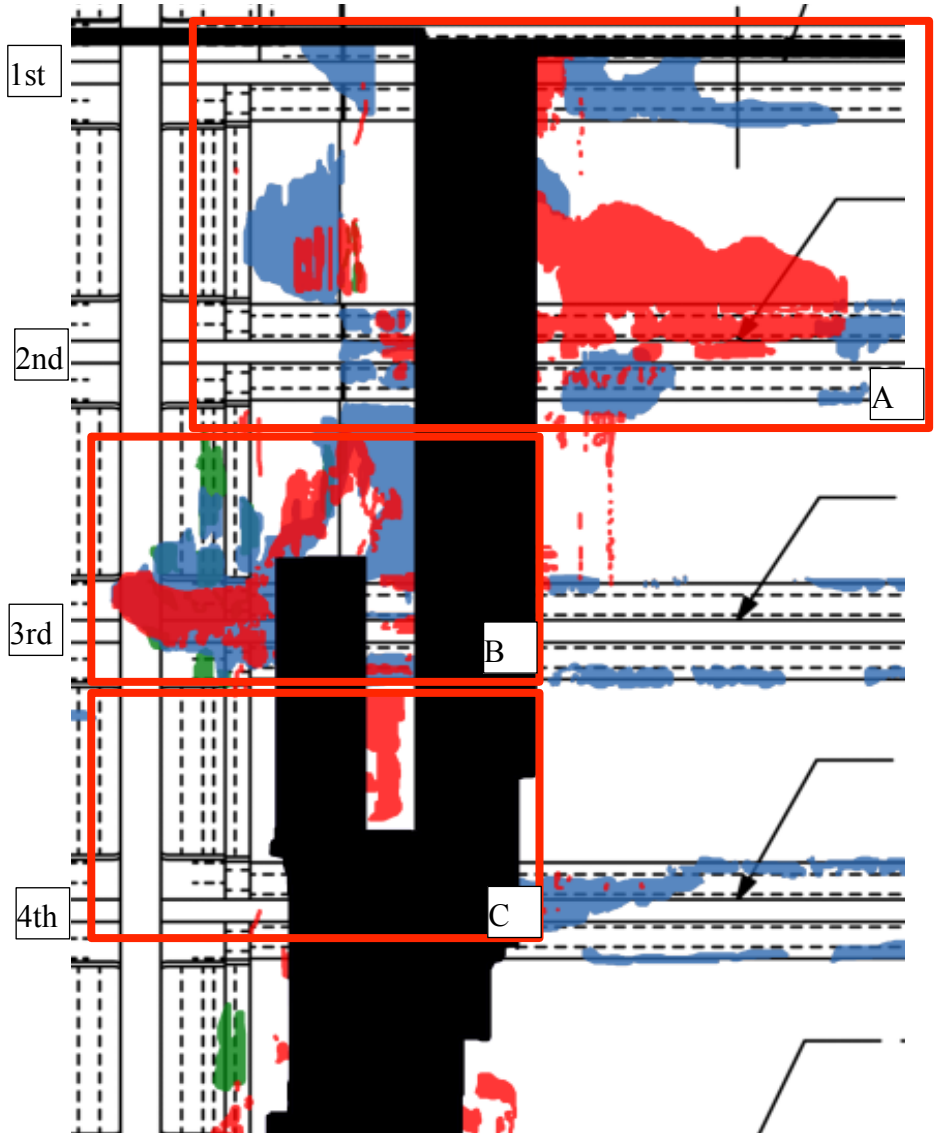

FIGURE 39. Detailed image of the upper portion of the forward bulkhead failure crack scans

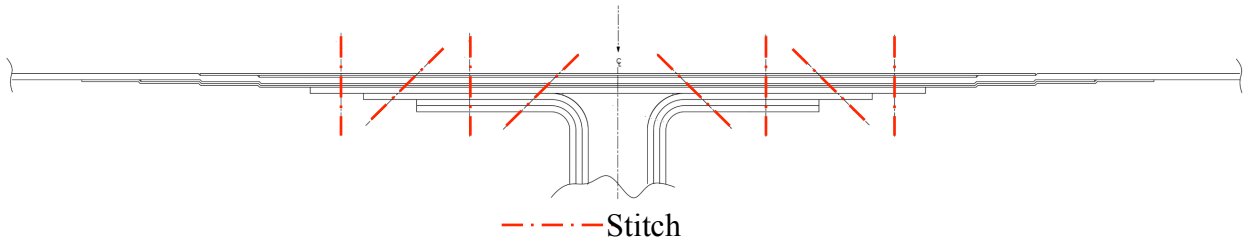

FIGURE 40. Detailed image of the cross section of a frame build up, showing the different stitch incident angles.

The first vertical crack ends and a horizontal crack seems to form at the flange of the 4th stringer (Fig. 39C), and extends until the ply build up area of the frame flange. At the tip of this horizontal crack a new vertical crack is shown extending up back into the 3rd stringer as well as down through the 4th 5th, and 6th stringer. The visible crack itself did not extend beyond the 7th stringer, which is located on the first of several built up layers that surround the forward porthole. The added stiffness of this ply build up between the 6th and 7th stringer created a much different delamination pattern (Fig. 41). In Fig. 41A the delaminations extend into the intersection of the frame and stringer flange but end at a stringer stitch row. In Fig. 41B massive subsurface delaminations in the skin region are shown, but they do not extend beyond the 1st and 2nd stitch line of the 7th stringer. Unfortunately, the horizontal extent of this damage was not captured in the scan area, but it can be extrapolated by scans further down (Fig. 41C) that the damage did not make it past the flanges of the frame.

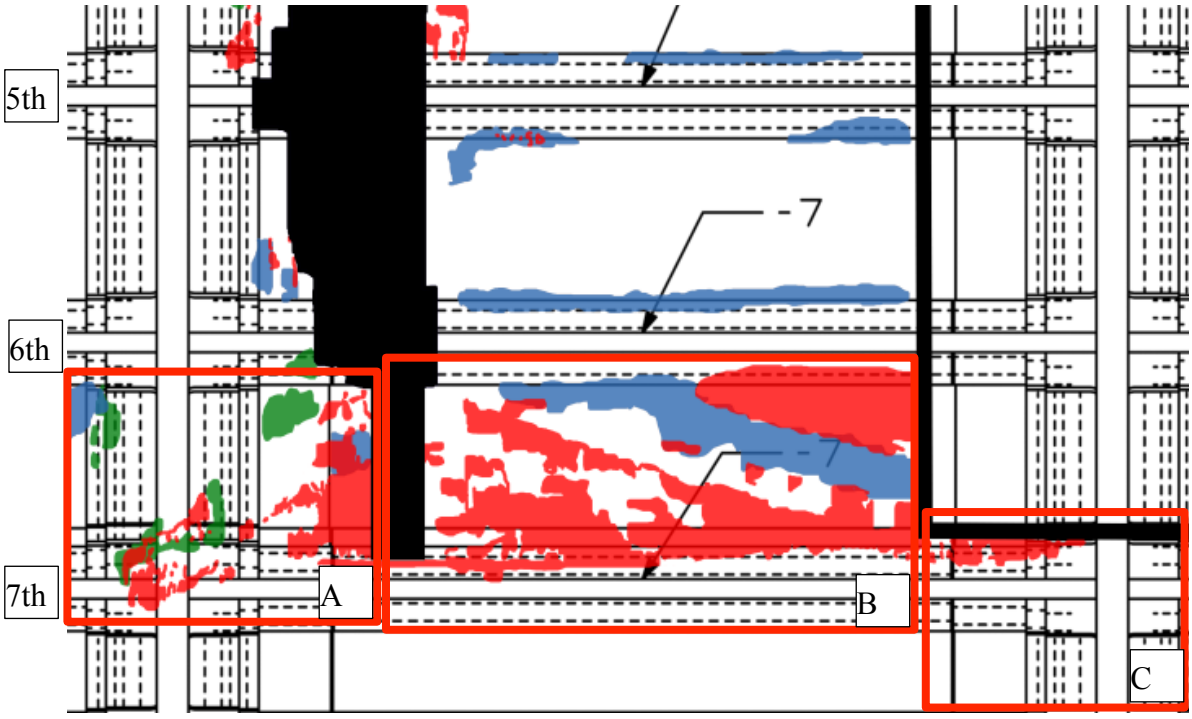

FIGURE 41. Detailed image lower section of the forward bulkhead failure crack scans.

There are a few characteristic delamination patterns that should be noted. First is the delamination growth along the interface between the skin and flange stitch line of the horizontal stringers (Fig. 42). This type of stitch line damage growth will be seen in many of the scans presented in this paper. There are some instances (such as the crown) where there are barely any stringers that didn't have this type of damage along the length. This damage is found between the inside skin to tear strap/stringer interface, and is usually confined to the 1st stitch of the flange, but can also be seen infiltrating into and stopping at the 2nd stitch line.

The damage-arresting stitching can be seen performing their purpose in several locations shown in the previous figures. In areas where stitching did fail on the forward bulkhead, it was often observed that the energy of a failed stitch violently rebounding back up against the surface was enough to break through the paint on the outer surface of the bulkhead, seen in Fig. 43.

Some anomalous damage can be observed to the leftmost side of the frame flange, seen in Figure Fig. 44. This damage seems to be mostly between the first unstitched frame flange buildup and the skin interface, and most of it seems to be contained at the first stitch line of the flange. While this may have be a result of the initial failure event, it is more likely secondary damage caused by the redistribution of forces that occurred afterward.

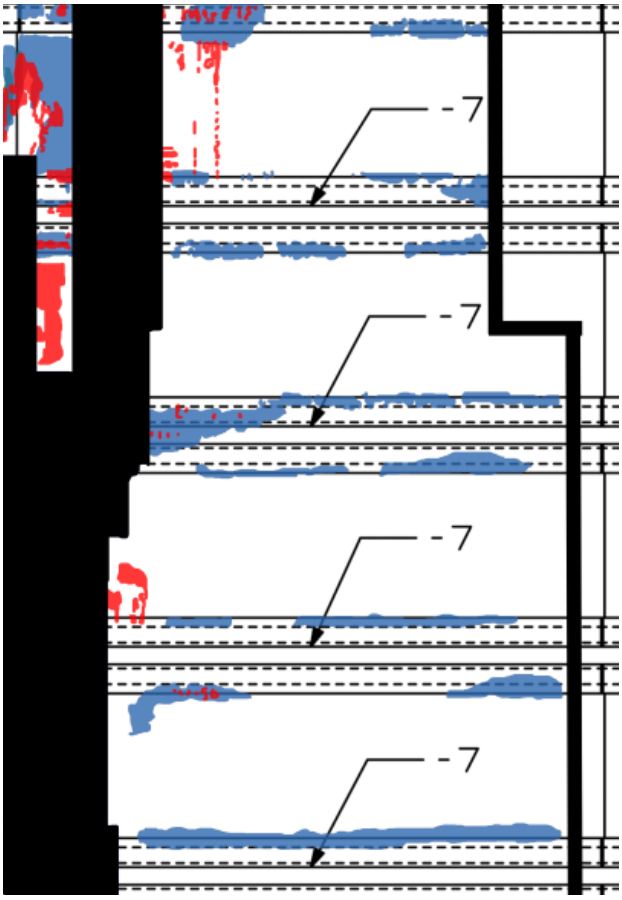

FIGURE 42. Detailed image showing the delaminations that have occurred in the first stitch line stringer/skin interface.

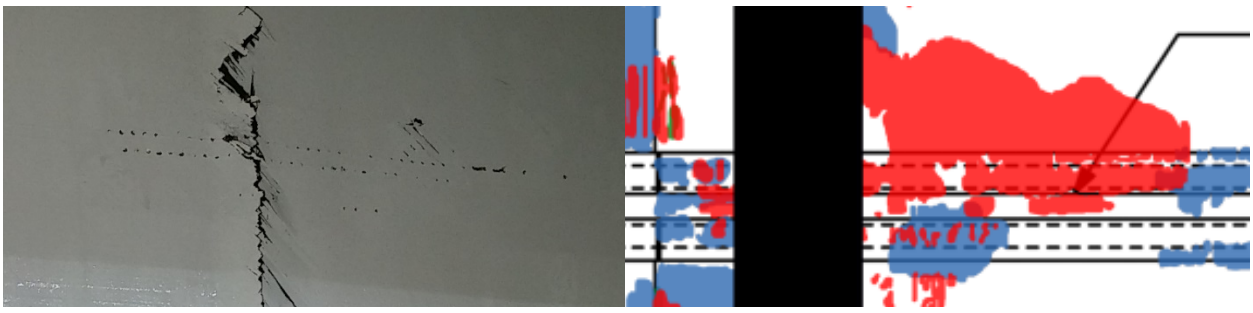

FIGURE 43. Photo of the surface damage caused by failed stitches rebounding against the surface, and the corresponding ultrasonic data.

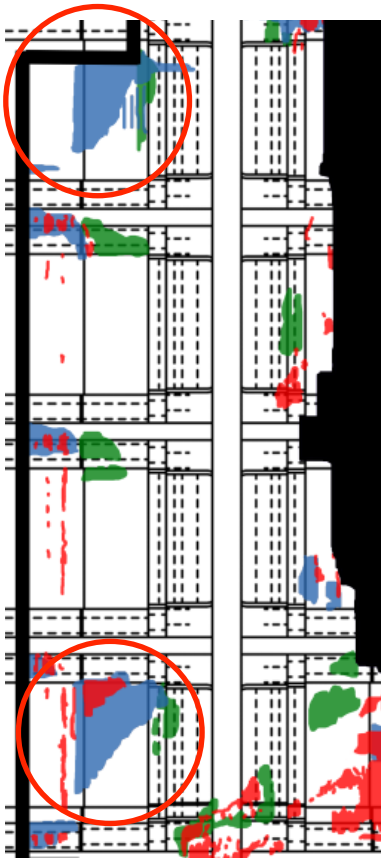

FIGURE 44. Image of anomalous delamination patterns on the opposite side of the vertical frame, shown inside the red circles.

4.3.5 Aft Bulkhead

The aft bulkhead failure crack is a continuation of the buckling and crack that formed on the starboard side of the crown, and is not directly connected to the saw cut at mid ship (Fig. 45). As stated earlier, the forward end of the buckling crack on the crown showed no visual indication of having spread to the forward bulkhead.

From the surface, the shape of the failure crack seems extend through the two uppermost stringers after it transitions from crown to bulkhead. At the third stringer a crack forms that is

parallel to the horizontal stringer. This crack ends at the ply buildup with the triangle geometry that supports the internal bay wall separator (Fig. 46), where another vertical crack forms that goes through an additional 4 stringers. The first scan section in this analysis was taken of the stringers that were located on the port side of the failure crack.

FIGURE 45. Photos showing the connection between the starboard side failure crack on the crown and the crack on the aft bulkhead.

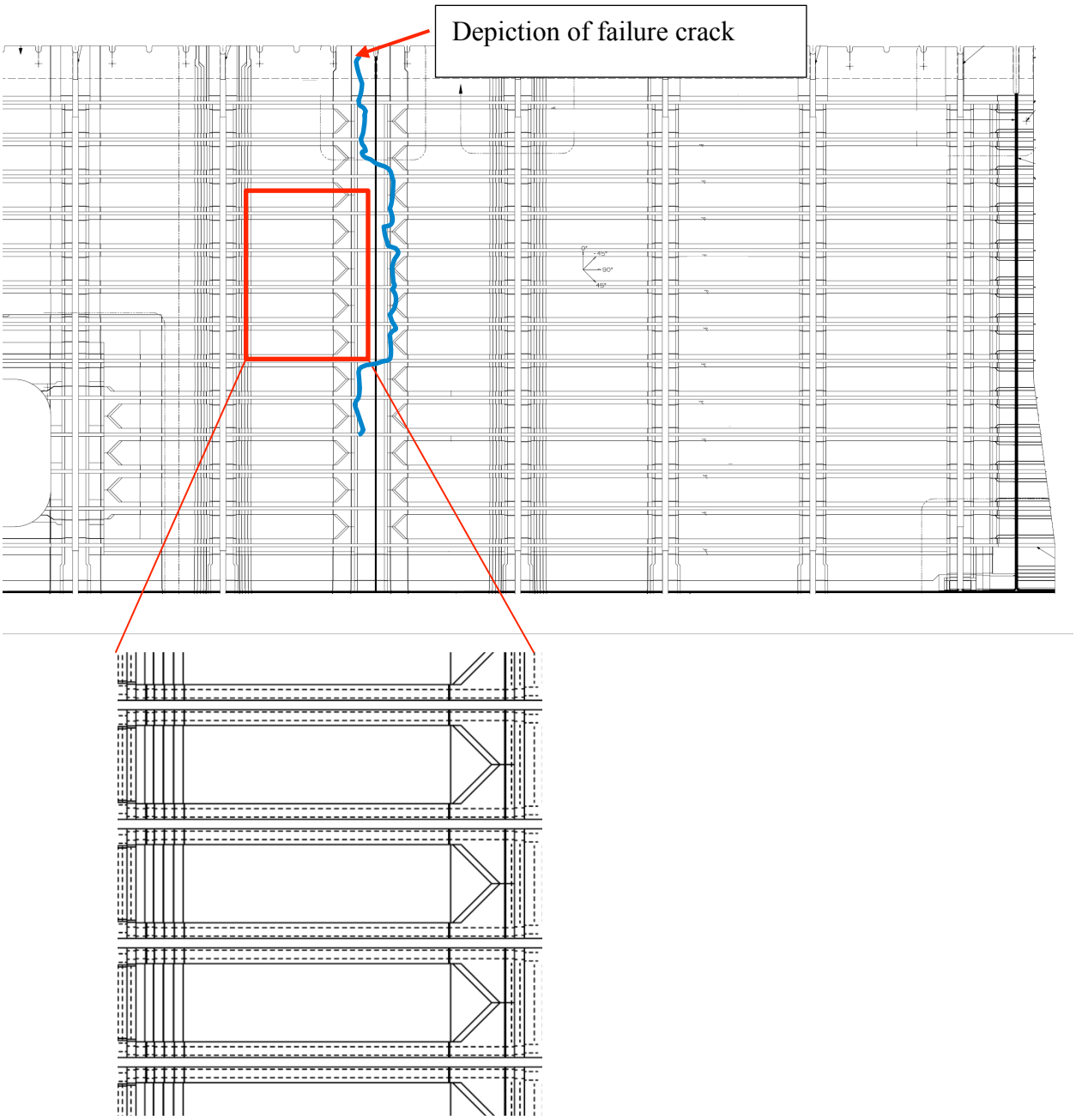

FIGURE 46. Location of the aft bulkhead failure crack in relation to the structure geometry.

The ultrasonic response was segmented at several depths, delaminations were located and traced, then mapped to the technical drawing, shown in (Fig. 47). Similarly to stringer scans seen in previous sections, there are clear signs of delamination between the skin layer and the tear strap of the stringers, and some subsurface skin delamination. This scan showed evidence of delamination between the stringer and its tear strap passing beneath the web of the stiffener as well as within the flanges. This is the place where this type of delamination was observed, as it did not appear in the scans of the forward bulkhead.

The second scan area on the aft bulkhead was located on the starboard side of the crack, parallel to the region shown in Fig. 47, which is shown in Fig. 48. This scan was constrained between the failure crack and a row of fasteners, which prevented the scanner from moving further.

In Fig. 49, the damage map of this scan is presented, rotated counter-clockwise by 90°. It is seen that the built-up corner geometry does a fair job of limiting the amount of delamination growth within the space between the stringers. The familiar delamination between the flange and the skin interface is still present, as well as deeper delaminations in the ply build up areas.

Unfortunately, while the bottom of the aft bulkhead failure crack was captured in the UT data, a fault in the scanning phased array probe casing resulted in signal artifacts, which made it very difficult to extract meaningful depth measurements from the data. However, the following was able to be determined: 1) the delamination damage went further than the surface crack would indicate, 2) the internal delaminations stopped at stitching of the next stringer down from where the surface crack stopped, and 3) first stitch line delaminations are seen on both sides of the stringer where the failure delamination was stopped.

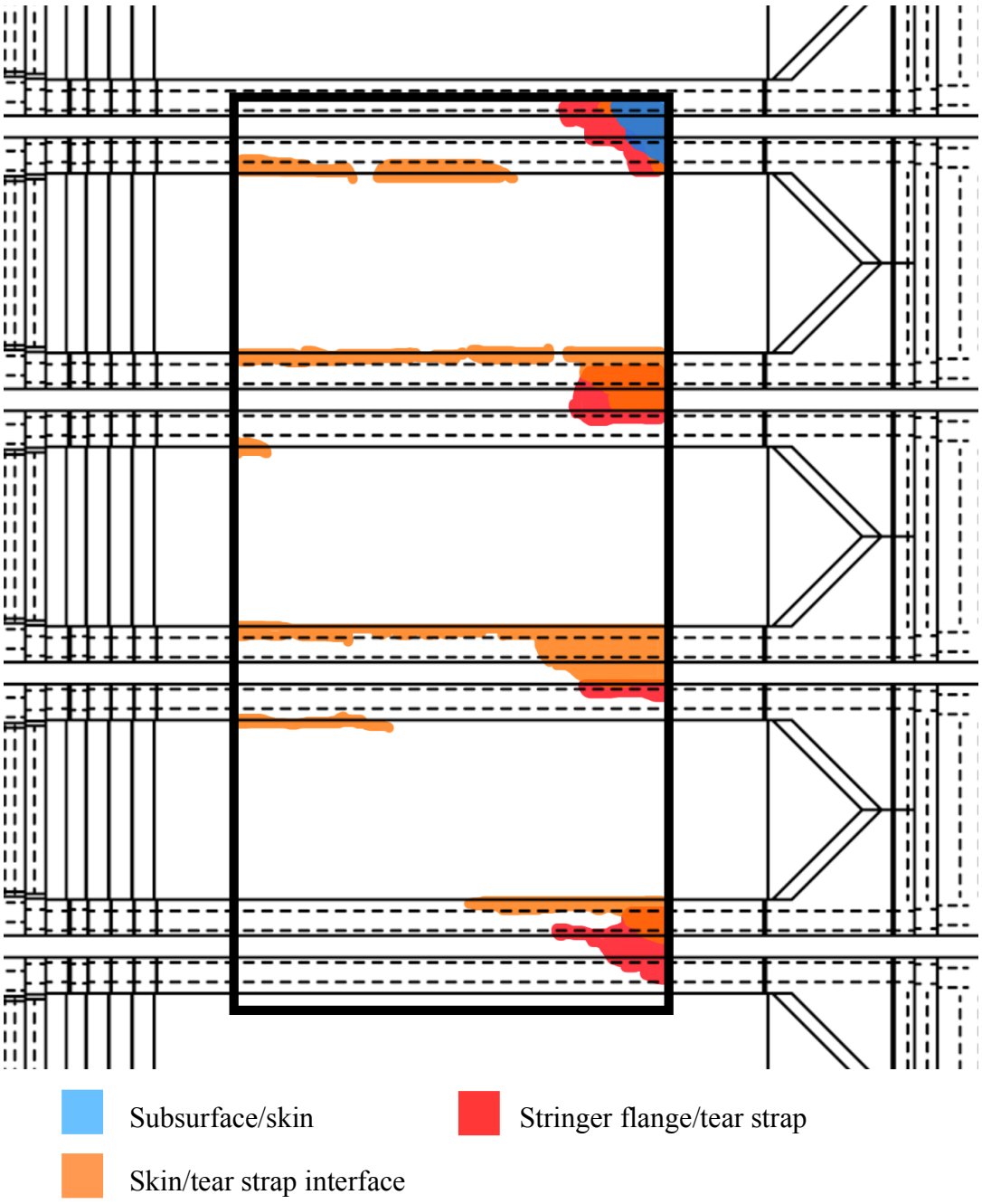

FIGURE 47. Damage map of a scanned section of the aft bulkhead. This section was located on the port side of the failure crack.

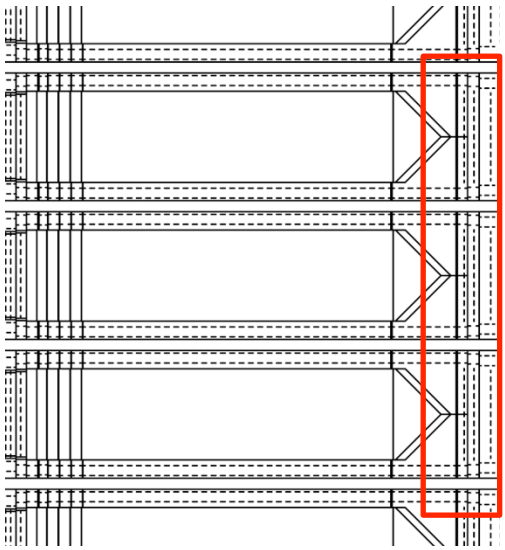

FIGURE 48. Location of the second scan area on the aft bulkhead.

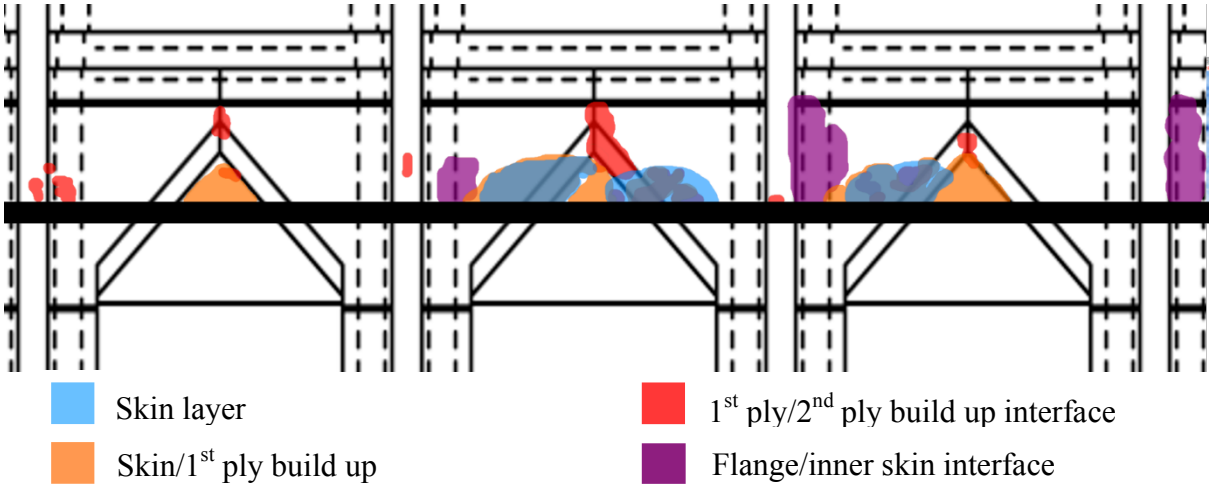

FIGURE 49. Damage map of the second scan area of the aft bulkhead.

5.0 Rod Push-Out Specimens

For the rod push-out study, a number of specimens were cut out of a larger PRSEUS panel, comprising 9-inch lengths of the overwrapped stiffener rod and a short length of the stiffener web. Pulse-echo ultrasonic NDE was performed on the overwrapped rods to screen for preexisting flaws or damage. No flaws were identified.

Eight rod specimens were subject to impact at the midpoint of the 9-inch length. These were rescanned ultrasonically to measure the extent of impact damage. C-scan images of these specimens arre presented in Fig. 50.

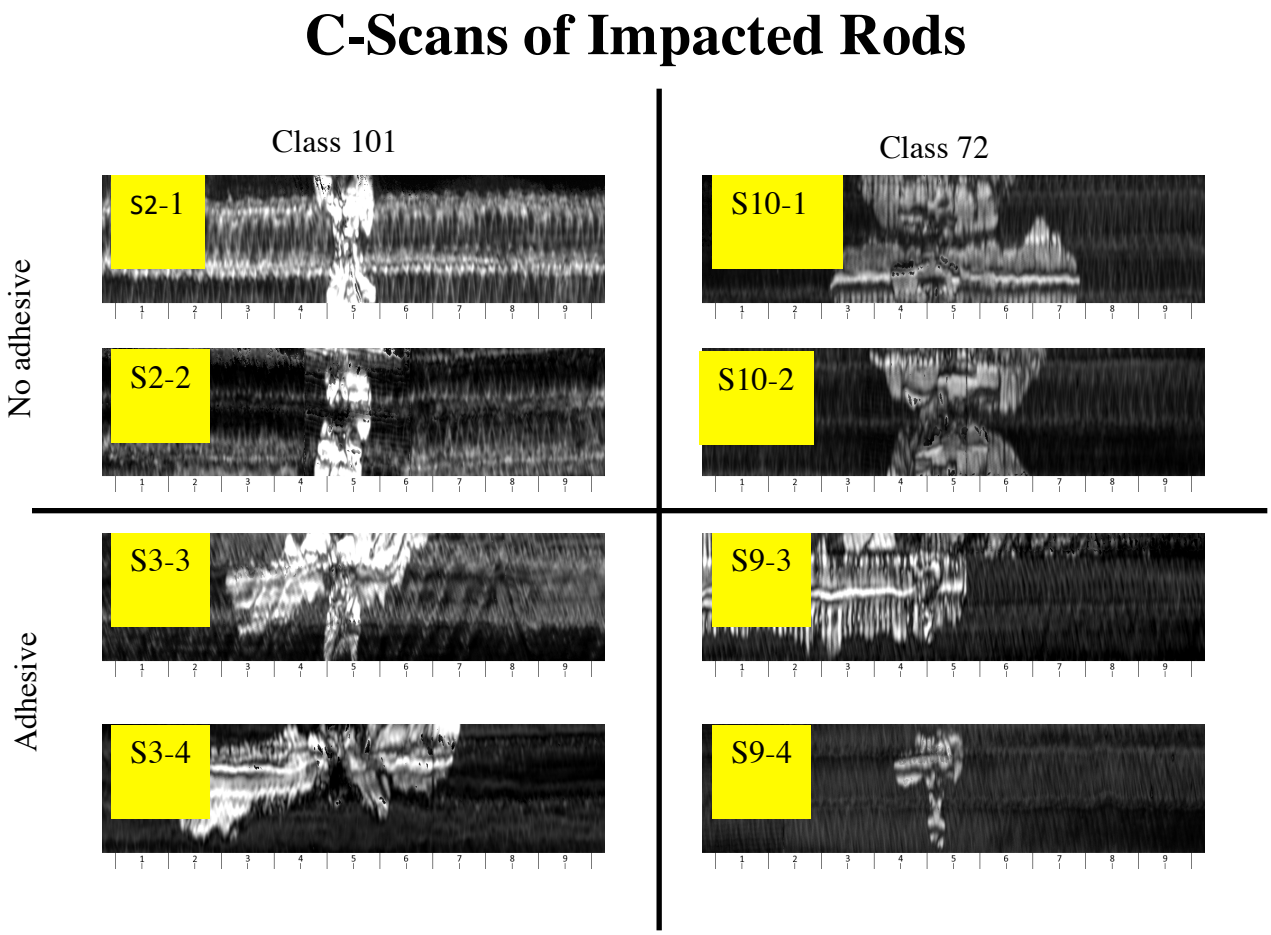

FIGURE 50. C-scans of impacted rod segments before cutting into push-out specimens.

The C-scan images were segmented into nine 1-inch wide areas, corresponding to the 1-inch long push-out specimens which were to be cut from the larger rod (Fig. 51). The fraction of the

area occupied by signals arising from delamination was measured, to serve as an index of the severity of damage. The results for the eight 9-inch long specimens are tabulated in Table 2.

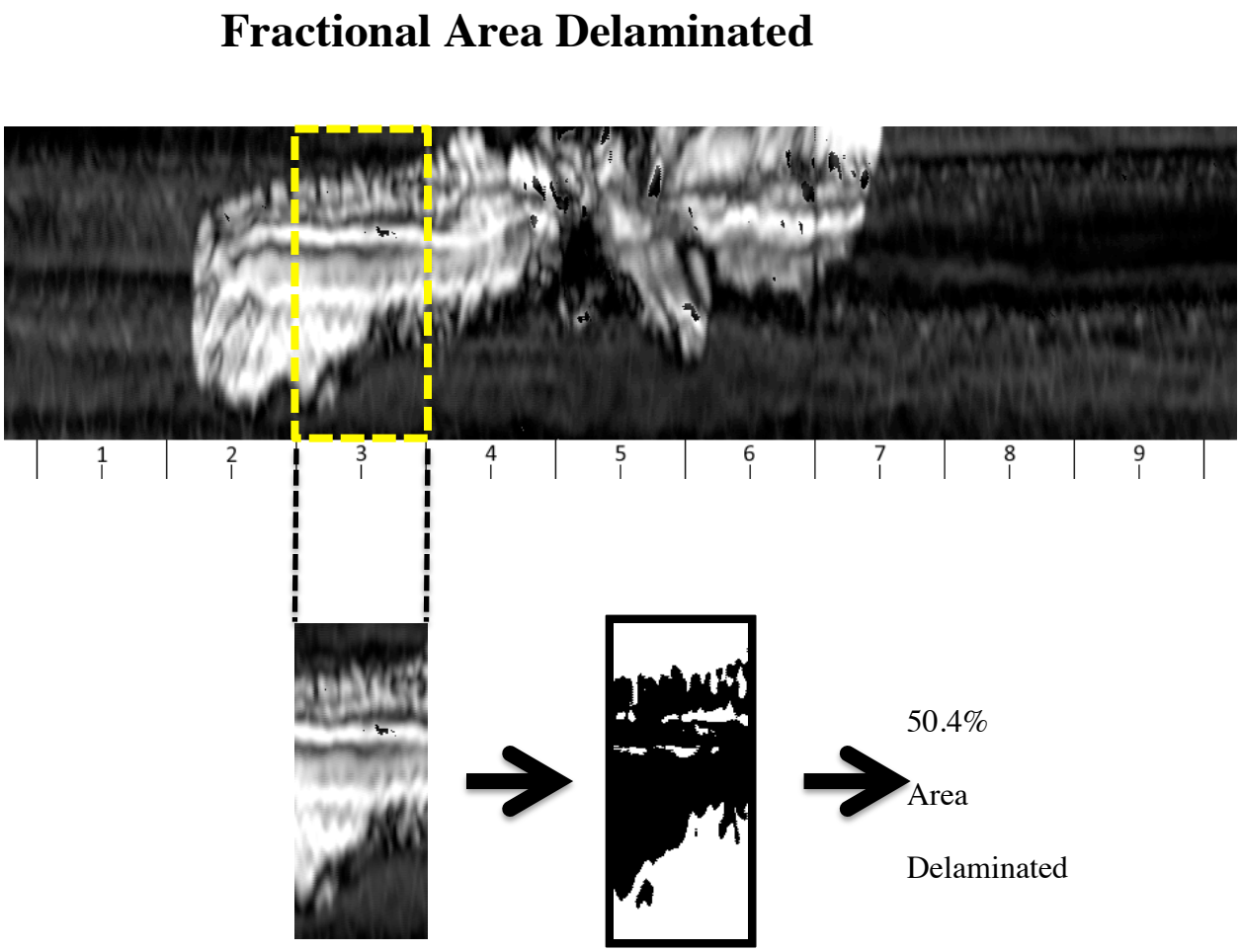

FIGURE 51. Example of the calculation of fractional area of delamination in a push-out specimen.

Percentage of Area Containing Delamination									
Specimen	Segment								
	1	2	3	4	5	6	7	8	9
S2-1	0.0	0.0	0.0	4.2	63.0	0.0	0.0	0.0	0.0
S2-2	0.0	0.0	0.0	7.7	40.2	1.2	0.0	0.0	0.0
S3-3	0.0	0.0	26.3	46.3	48.1	24.1	0.0	0.0	0.0
S3-4	0.0	45.4	49.4	43.2	29.1	41.5	14.6	0.0	0.0
S9-3	61.7	55.8	63.7	54.0	32.3	0.0	0.0	0.0	0.0
S9-4	0.0	0.0	0.0	12.3	24.9	0.0	0.0	0.0	0.0
S10-1	0.0	0.0	33.1	76.5	75.8	60.8	41.0	0.0	0.0
S10-2	0.0	0.0	0.6	36.6	51.6	45.4	3.3	0.0	0.0

TABLE 2. Table of inspection sites and points during the test sequence measurements were made.

6.0 Conclusion

One of the key performance expectations of the PRSEUS structural concept is that the stitches in the stiffeners and frames would serve to constrain damage growth during service. Over the course of a building block development program, evidence provided by NDE measurements indicates that the stitches in PRSEUS performed very well toward this expectation, all the way to constraining the growth of damage adjacent to failure cracks during catastrophic structural failure of large-scale test articles.

7.0 Acknowledgements

The authors wish to acknowledge the important contribution by Jeffrey P. Seebo (Analytical Mechanics Associates, Inc., Hampton, Virginia 23666) to the acquisition of the NDE data on the MBB test article. We also acknowledge Mr. Seebo and Joshua Brown (National Institute of Aerospace, Hampton, Virginia 23666) for designing and constructing the captive water column for a curved phased array probe. Finally, we acknowledge Patricia Howell (NASA Langley Research Center) for contributing to data acquisition on the MBB.

8.0 References

1. Boeing Document ZA153342, Rev. B, HWB Multi-Bay Test Article: Test Specification, (2014).

2. A. Velicki, K. Linton, K. Hoffman, P. Thrash, R. Pickell, and R. Turley, “Fabrication of Lower Section and Upper Forward Bulkhead Panels of the Muti-Bay Box and Panel Preparation.” NASA/CR-2015-218981, (2015).

3. D. Jegley, M. Rouse, A. Przekop, and A. Lovejoy, “The Behavior of a Stitched Composite Large-Scale Multi-Bay Ptressure Box,” NASA/TM-2016-218972 (2016).

4. A. Przekop and H. T. Wu, “Test Analysis Correlation for a Large-Scale Pressurized Stitched Composite Multi-Bay Box,” NASA/TM-2016-218973 (2016).

5. Michael R. Horne, "Evaluation of Acoustic Emission SHM of PRSEUS Multi-Bay Box Tests,” NASA/TM-2015-218976 (2015).

6. Jason P. Moore, Adam Przekop, Peter D. Juarez, and Mark C. Roth, "Fiber Optic Rosette Strain Gauge Development and Application on a Large-scale Composite Structure,” NASA/TM-2015-218970 (2015).

7. Andrew E. Lovejoy, “T-Cap Pull-Off and Bending Behavior for Stitched Structure,” NASA/TM-2016-218970 (2016).

8. F. Leone, “Rod Push-Out Behavior for PRSEUS Specimens,” NASA/TM-2016-218975 (2016).

9. F. Leone and D. Jegley, “Compression Testing of Stitched Single Stiffener Specimens,” NASA/TM-2016-218974 (2016).

10. A. Velicki, "Damage Arresting Composites for Shaped Vehicles," NASA-CR-2009-215932, (2009).

11. D. Jegley, “Experimental Behavior of Fatigued Single Stiffener PRSEUS Specimens,” NASA-TM-2009-215955, (2009).

12. Patrick H. Johnston, “Pulse-Echo Phased Array Ultrasonic Inspection of Pultruded Rod Stitched Efficient Unitized Structure (PRSEUS),” Review of Progress in Quantitative Nondestructive Evaluation, vol 30, AIP Conf. Proc. 1335, pp. 1432-1439 (2011).

13. D. C. Jegley, Proceed. Soc. of Exper. Mech. Conf., Mohegan Sun, Uncasville, CT (2011).

14. A. Bergan, *et al*, 2nd Annual Aircraft Airworthiness & Sustainment Conference (2011).

15. Nicolette Yovanof, Andrew E. Lovejoy, Jaime Baraja and Kevin Gould, "Design, Analysis and Testing of a PRSEUS Pressure Cube to Investigate Assemby Joints," 3rd Annual Aircraft Airworthiness and Sustainment Conference, Baltimore, MD, April, 2012.

16. John T. Wang, Ray W. Grenoble and Robert D. Pickell, "Structural Integrity Testing Method for PRSEUS Rod-Wrap Stringer Design," 53rd AIAA/ASME/ASCE/AHS/ASC Structures, Structural Dynamics and Materials Conference. 23-26 April 2012, Honolulu, Hawaii.

17. Patrick H. Johnston, "Ultrasonic Nondestructive Evaluation of PRSEUS Pressure Cube Article in Support of Load Test to Failure," NASA/TM-2013-217799.

18. Boeing Document ZA153690, Pressure Cube Test Specification, (2011).

19. Andrew E. Lovejoy, "PRSEUS Pressure Cube Test Data and Response," NASA/TM-2013-217795.

20. Michael R. Horne and Eric I. Madaras, "Evaluation of Acoustic Emission SHM of PRSEUS Composite Pressure Cube Tests," NASA/TM-2013-217993.

21. Patrick H. Johnston and F. Raymond Parker, "NDE Evidence for the Damage Arrestment Performance of PRSEUS Composite Cube During High-Pressure Load Test," Review of Progress in Quantitative Nondestructive Evaluation, vol 33A, AIP Conf. Proc. 1581, pp. 1106-1113 (2014).

22. Ambur, D. A., Rouse, M., Starnes, J. H., and Shuart, M. J., "Facilities for Combined Loads Testing of Aircraft Structures to Satisfy Structural Technology Development Requirements," 5th NASA/DoD Advanced Composites Technology Conference, Seattle, WA, August 22-25, 1994.

REPORT DOCUMENTATION PAGE

Form Approved
OMB No. 0704-0188

1. REPORT DATE *(DD-MM-YYYY)*	2. REPORT TYPE	3. DATES COVERED *(From - To)*
01-05-2016	Technical Memorandum	

4. TITLE AND SUBTITLE

Ultrasonic Nondestructive Evaluation of Pultruded Rod Stitched Efficient Unitized Structure (PRSEUS) During Large-Scale Load Testing and Rod Push-Out Testing

5a. CONTRACT NUMBER

5b. GRANT NUMBER

5c. PROGRAM ELEMENT NUMBER

6. AUTHOR(S)

Johnston, Patrick H.; Juarez, Peter D.

5d. PROJECT NUMBER

5e. TASK NUMBER

5f. WORK UNIT NUMBER

338881.02.22.07.01.01

7. PERFORMING ORGANIZATION NAME(S) AND ADDRESS(ES)

NASA Langley Research Center
Hampton, VA 23681-2199

8. PERFORMING ORGANIZATION REPORT NUMBER

L-20709

9. SPONSORING/MONITORING AGENCY NAME(S) AND ADDRESS(ES)

National Aeronautics and Space Administration
Washington, DC 20546-0001

10. SPONSOR/MONITOR'S ACRONYM(S)

NASA

11. SPONSOR/MONITOR'S REPORT NUMBER(S)

NASA-TM-2016-218978

12. DISTRIBUTION/AVAILABILITY STATEMENT

Unclassified - Unlimited
Subject Category 71
Availability: NASA STI Program (757) 864-9658

13. SUPPLEMENTARY NOTES

14. ABSTRACT

The Pultruded Rod Stitched Efficient Unitized Structure (PRSEUS) is a structural concept developed by the Boeing Company to address the complex structural design aspects associated with a pressurized hybrid wing body (HWB) aircraft configuration. The HWB has long been a focus of NASA's environmentally responsible aviation (ERA) project, following a building block approach to structures development, culminating with the testing of a nearly full-scale multi-bay box (MBB), representing a segment of the pressurized, non-circular fuselage portion of the HWB. PRSEUS is an integral structural concept wherein skins, frames, stringers and tear straps made of variable number of layers of dry warp-knit carbon-fiber stacks are stitched together, then resin-infused and cured in an out-of-autoclave process. The PRSEUS concept has the potential for reducing the weight and cost and increasing the structural efficiency of transport aircraft structures. A key feature of PRSEUS is the damage-arresting nature of the stitches, which enables the use of fail-safe design principles. During the load testing of the MBB, ultrasonic nondestructive evaluation (NDE) was used to monitor several sites of intentional barely-visible impact damage (BVID) as well as to survey the areas surrounding the failure cracks after final loading to catastrophic failure. The damage-arresting ability of PRSEUS was confirmed by the results of NDE. In parallel with the large-scale structural testing of the MBB, mechanical tests were conducted of the PRSEUS rod-to-overwrap bonds, as measured by pushing the rod axially from a short length of stringer.

15. SUBJECT TERMS

Composites; NDE; Stitched; Ultrasonic

16. SECURITY CLASSIFICATION OF:			17. LIMITATION OF ABSTRACT	18. NUMBER OF PAGES	19a. NAME OF RESPONSIBLE PERSON
a. REPORT	b. ABSTRACT	c. THIS PAGE			STI Help Desk (email: help@sti.nasa.gov)
					19b. TELEPHONE NUMBER *(Include area code)*
U	U	U	UU	66	(757) 864-9658